



HAL
open science

The Global Land Carbon Cycle Simulated With ISBA-CTRIP: Improvements Over the Last Decade

Christine Delire, Roland S  f  rian, Bertrand Decharme, Ramdane Alkama,
Jean-christophe Calvet, Dominique Carrer, Anne-laure Gibelin, Emilie
Joetzjer, Xavier Morel, Matthias Rocher, et al.

► To cite this version:

Christine Delire, Roland S  f  rian, Bertrand Decharme, Ramdane Alkama, Jean-christophe Calvet, et al.. The Global Land Carbon Cycle Simulated With ISBA-CTRIP: Improvements Over the Last Decade. *Journal of Advances in Modeling Earth Systems*, 2020, 12 (9), 10.1029/2019MS001886 . hal-03419707

HAL Id: hal-03419707

<https://hal.science/hal-03419707>

Submitted on 18 Nov 2021

HAL is a multi-disciplinary open access archive for the deposit and dissemination of scientific research documents, whether they are published or not. The documents may come from teaching and research institutions in France or abroad, or from public or private research centers.

L'archive ouverte pluridisciplinaire **HAL**, est destin  e au d  p  t et    la diffusion de documents scientifiques de niveau recherche, publi  s ou non,   manant des   tablissements d'enseignement et de recherche fran  ais ou   trangers, des laboratoires publics ou priv  s.



Distributed under a Creative Commons Attribution - NonCommercial - NoDerivatives 4.0
International License



RESEARCH ARTICLE

10.1029/2019MS001886

Special Section:The CNRM Climate and Earth
System Models for CMIP6

The Global Land Carbon Cycle Simulated With ISBA-CTRIP: Improvements Over the Last Decade

Christine Delire¹ , Roland S  f  rian¹ , Bertrand Decharme¹ , Ramdane Alkama² ,
Jean-Christophe Calvet¹, Dominique Carrer¹, Anne-Laure Gibelin³, Emilie Joetzjer¹ ,
Xavier Morel¹ , Matthias Rocher¹, and Diane Tzanos¹

¹CNRM, Centre National de Recherches M  t  orologiques, UMR3589 Universit   de Toulouse/M  t  o-France/CNRS, Toulouse, France, ²European Commission, Joint Research Center, JRC, Ispra, Italy, ³Direction des Services M  t  orologiques, M  t  o-France, Toulouse, France

Key Points:

- This paper documents the updates to the biogeochemical module of the ISBA-CTRIP land surface system for use in the CNRM-ESM 2-1 Earth system model
- The newly represented processes are the leaching of carbon and transport of dissolved organic carbon to the ocean, fire with area burned and carbon emissions, and land cover changes
- The largest improvements in the representation of net primary productivity are due to improved autotrophic respiration

Supporting Information:

- Supporting Information S1

Correspondence to:

C. Delire,
christine.delire@meteo.fr

Citation:

Delire, C., S  f  rian, R., Decharme, B., Alkama, R., Calvet, J.-C., Carrer, D., et al. (2020). The global land carbon cycle simulated with ISBA-CTRIP: Improvements over the last decade. *Journal of Advances in Modeling Earth Systems*, 12, e2019MS001886. <https://doi.org/10.1029/2019MS001886>

Received 9 SEP 2019

Accepted 17 APR 2020

Accepted article online 20 APR 2020

Abstract We present the latest version of the ISBA-CTRIP land surface system, focusing on the representation of the land carbon cycle. We review the main improvements since the year 2012, mainly added modules for wild fires, carbon leaching through soil and transport of dissolved organic carbon to the ocean, and land cover changes but also improved representation of photosynthesis, respiration, and plant functional types. This version of ISBA-CTRIP is fully described in terms of land carbon pools, fluxes, and their interactions. Results are compared with the previous version in an off-line mode forced by observed climate during the historical time period. The two simulations are presented to demonstrate the model performance compared to an ensemble of observed and observation-derived data sets for gross and net primary productivity, heterotrophic and autotrophic respiration, above and below ground biomass, litter, and soil carbon pools. New developments specific to the new version such as burned area, fire emissions, carbon leaching, and land cover are also validated against observations. The results show clearly that the latest version of ISBA-CTRIP outperforms the former version and reproduces generally well the observed mean spatial patterns in carbon pools and fluxes, as well as the seasonal cycle of leaf area index. The trends of the global fluxes over the last 50 years agree with other global models and with available estimates. This comparison gives us confidence that the model represents the main processes involved in the terrestrial carbon cycle and can be used to explore future global change projections.

Plain Language Summary The land surface exchanges energy, water, and carbon with the atmosphere and partly controls the atmospheric CO₂ concentration. It is therefore crucial to represent correctly the carbon cycle on land in models designed to be used in Earth System Models. We present here the improvements made to the representation of the land carbon cycle by the land surface system ISBA-CTRIP. We improved the representation of several processes using published data, and we added processes that were not represented. The new version of the model performs better than the previous one at representing the carbon fluxes and pools, when compared to a series of observation data sets. This evaluation suggests that we can use ISBA-CTRIP to explore the changing climate and carbon cycle.

1. Introduction

Land surface models were developed in order to represent the energy, momentum, and mass exchange processes taking place at the land surface (Pitman, 2003) in climate and weather forecasting models. Their complexity and the number of process represented have increased through time since the pioneering work of Manabe (1969), Charney et al. (1975), or Deardorff (1977, 1978), but they differ greatly in the choice of processes included and in the degree of complexity used to represent each process. Coupled to atmosphere-ocean models, they take part in the Climate Model Intercomparison Project (CMIP) to simulate the past and future climate that is used in the successive Assessment Reports of the United Nations Intergovernmental Panel on Climate Change (IPCC). Land surface models are also used to complement missing data and estimate processes over large spatial scales, not available to in situ measurements. The Global Carbon Project (Le Qu  r   et al., 2018) for instance presents for every year since 1959 a complete global carbon budget using land surface/vegetation models to estimate the global land carbon sink.

  2020. The Authors.

This is an open access article under the terms of the Creative Commons Attribution-NonCommercial-NoDerivs License, which permits use and distribution in any medium, provided the original work is properly cited, the use is non-commercial and no modifications or adaptations are made.

Interaction Soil-Biosphere-Atmosphere (ISBA) (Noilhan & Planton, 1989) is the land surface model developed at the research center (Centre National de Recherches Météorologiques; <https://www.umr-cnrm.fr/>) of the French weather forecasting service (Météo-France). It is tied to the Total Runoff Integrating Pathways (TRIP) river routing model (Oki & Sud, 1998) to calculate river discharges up to the ocean from the ISBA-computed total runoff. The ISBA-TRIP land surface system (Decharme & Douville, 2007) was included in the SURFEX numerical interface (Masson et al., 2013; available freely at <https://www.umr-cnrm.fr/surfex/>), designed to ease both the coupling of ISBA-TRIP (and the ocean model) to all atmospheric models of Météo-France and its use in off-line model. ISBA-TRIP was the land surface system of CNRM's climate model, CNRM-CM5 (Voldoire et al., 2013), developed to participate to the Fifth Assessment Report (AR5) of the IPCC. In parallel, CNRM developed its first Earth System Model CNRM-ESM 1 (Séférian et al., 2016) sharing all the physical components of CNRM-CM5 but including a version of ISBA that represents the cycling of carbon between the atmosphere, the land vegetation, and the soil.

The version of ISBA with carbon cycling (Calvet, 2000; Calvet et al., 1998) was used to study the effect of drought in the Amazon Basin (Joetzjer et al., 2014; Joetzjer et al., 2015) and the Northern Hemisphere permafrost carbon vulnerability (McGuire et al., 2016; Rawlins et al., 2015; Xia et al., 2017). The off-line studies on the Amazon Basin and the results from CNRM-ESM 1 showed some important shortcomings. The model for instance overestimated forest productivity globally and tree respiration in the tropics. It did not take into account land use and land cover changes although numerous papers showed with models (see for instance Pitman et al., 2009; Pielke et al., 2011) and with data (Alkama & Cescatti, 2016) their importance on the climate system in terms of biophysics and biogeochemistry. Similarly, fires were not represented despite their role in the climate system through emissions of carbon species and aerosols, changes in vegetation, and soil biogeochemistry (Pellegrini et al., 2017) but also their direct role on the physical climate through changes in land surface properties, notably albedo (see for instance Rocha et al., 2012; Bonan, 2008, or Randerson et al., 2006). These shortcomings prompted a thorough update of the biogeochemical module of ISBA-CTRIP. In parallel, the land surface physics was also thoroughly upgraded (14 layer-discretized solution of the energy and water balance in soils, 12-layer snow model, etc.; see Decharme et al., 2019). The resulting model serves as the land surface component of CNRM-ESM 2-1 (Séférian et al., 2019), the Earth system of second generation developed by CNRM-CERFACS for the sixth Coupled Model Intercomparison Project (CMIP6; Eyring et al., 2016).

The first goal of this study is to present the new version of ISBA-CTRIP, focusing on the changes that concern the land carbon cycle: mainly the added modules for wild fires, carbon leaching through soil and transport of dissolved organic carbon (DOC) to the ocean, and land cover changes, but also improved representation of photosynthesis, respiration, and plant functional types (PFTs). The second goal is to describe the performance of ISBA-CTRIP at replicating present-day observations and track to what extent improved or newly represented processes impact the skill of ISBA-CTRIP. We focus on the mean state and the trends. In the remainder of the document, we refer to the new version of ISBA-CTRIP as “ISBA_bgc6” and “ISBA_bgc5” for the old. Section 2 is devoted to the description of the model focusing on the changes between versions. Section 3 describes the simulation design and the observations used for evaluation. The results are presented and discussed in section 4, followed by a brief summary and conclusions in section 5.

2. Model Description: ISBA_bgc6 in Comparison to ISBA_bgc5

We here describe the latest version of the biogeochemical module (see Figure 1) that is used in the CMIP6 exercise, especially in CNRM-ESM 2-1 (Séférian et al., 2019), stressing the differences with the module that was used in CNRM-ESM 1. These changes are summarized in Table 1. The changes made in the land surface physics and hydrology modules between CMIP5 and CMIP6 are described in Decharme et al. (2019) and we only give here a brief summary.

The land surface physics module of ISBA (Noilhan & Planton, 1989; Noilhan & Mahfouf, 1996) computes the exchange of water and energy between the land surface and the atmosphere. In this version of the module, energy and water balances are solved for one vegetation canopy, 12 snow layers and up to 14 soil layers where soils are deep. The energy and water balances are influenced by soil texture, soil albedo, and soil carbon content. Evapotranspiration results from the direct evaporation of canopy-intercepted rainfall, from bare soil evaporation and from vegetation transpiration controlled by stomatal conductance (see below). In contrast

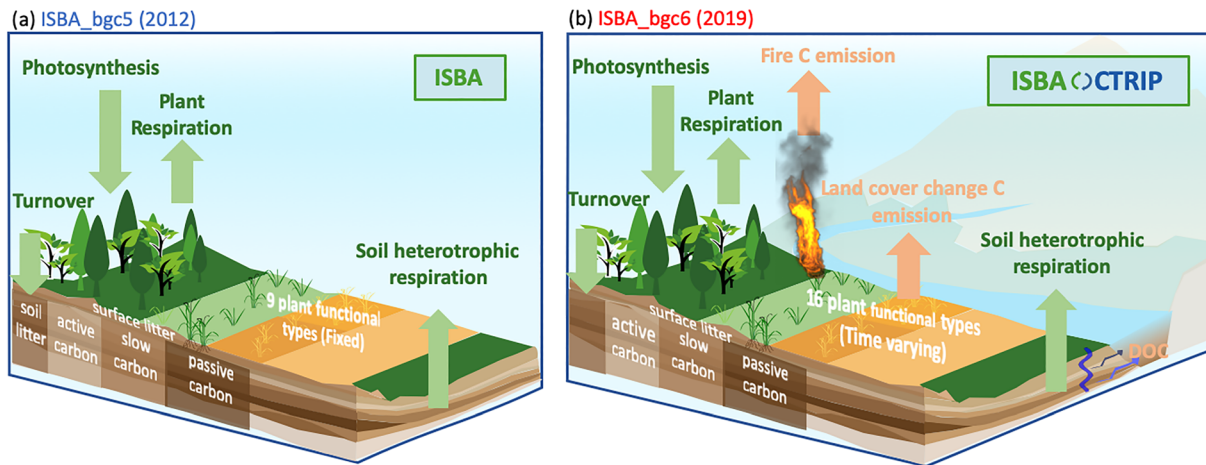


Figure 1. Scheme of the biogeochemical modules in ISBA in its 2012 version (ISBA_bgc5) and 2019 version (ISBA_bgc6). (a) ISBA_bgc5 represented vegetation photosynthesis leading to gross primary productivity (GPP), autotrophic respiration (R_a), vegetation mortality as turnover processes, and heterotrophic respiration resulting from the decomposition of litter and soil organic matter, for nine fixed plant functional types (PFTs). (b) ISBA_bgc6 has an improved representation of GPP and R_a for 16 PFTs whose area change yearly according to land cover change data. The carbon flux resulting from the land cover change is called fLCC. ISBA_bgc6 also has a fire module that calculates area burned and carbon emissions (fire C). Finally, ISBA_bgc6 has a simple representation of dissolved organic carbon (DOC) leaching through the soil and transported to the ocean.

to most land surface models, ISBA with its river routing module CTRIP includes a representation of aquifers (Vergnes & Decharme, 2012) that feed back on soil moisture content. It also represents inundation from rivers in floodplains. A detailed description of the snow module is given in Decharme et al. (2016). A detailed study of the land surface physics and hydrology, including the effects of aquifers and inundation on the surface energy and water budgets, is presented in Decharme et al. (2019).

The land biogeochemical module in ISBA represents plant physiology (photosynthesis and respiration), carbon allocation and turnover, and carbon cycling through litter and soil (Calvet et al., 1998; Calvet & Soussana, 2001; Gibelin et al., 2006, 2008). Carbon assimilation is calculated from air CO_2 concentration, leaf temperature, and solar radiation considering C3 or C4 photosynthetic pathways.

2.1. Photosynthesis

Photosynthesis is represented by the semiempirical model proposed by Jacobs (1994), based on Goudriaan et al. (1985) and implemented by Calvet et al. (1998). It uses the concept of mesophyll conductance defined in this framework as the rate of photosynthesis under light-saturated conditions (Jacobs, 1994). As such, this scheme does not explicitly account for the Michealis-Menten kinetics of the Rubisco enzyme formalized by

Table 1
Main Characteristics of ISBA_bgc5 and ISBA_bgc6

Processes	ISBA_bgc5	ISBA_bgc6
Land surface physics	Decharme et al. (2019)	Decharme et al. (2019)
Vegetation description	9 PFTs, rock, ice, desert	16 PFTs, rocks, ice, desert
Land cover changes	No	Yes, annual net changes
Vegetation dynamics	No	No
Photosynthesis	Goudriaan et al. (1985), Jacobs (1994)	Goudriaan et al. (1985), Jacobs (1994) with updated parameters
Hydraulic stress	Calvet (2000), Calvet et al. (2004)	Calvet (2000), Calvet et al. (2004), except for tropical forest (Joetzier et al., 2015)
Respiration	Goudriaan et al. (1985) and Jacobs (1994)	Goudriaan et al. (1985) and Jacobs (1994) Vertical profile of leaf respiration for tree canopies, Added sapwood respiration
Radiative transfer	Goudriaan's (1986) 3-point Gaussian solution	10-layer scheme with direct and diffuse radiation (Carrer et al., 2013)
Specific leaf area	Dependent on leaf N	Dependent on leaf N and dependence on CO_2 concentration
CO_2 downregulation	No	Following Arora et al. (2009)
Fire	No	Based on GlobFirm (Thonicke et al., 2001)
DOC/soil C leaching	No	Simple parameterization

Farquhar et al. (1980) and Collatz et al. (1992). Goudriaan's approach was originally chosen by Calvet et al. (1998) because it uses conductances instead of enzyme kinetics and was conceptually closer to what was used at the time in the land surface modeling community. Goudriaan's approach has the advantage of being fairly simple, but its parameters are rarely measured by the ecophysiology community. Here, we show how we recently related Goudriaan's main parameters to Farquhar's model to be able to use the ecophysiology body of science and the TRY database in particular (Kattge et al., 2011).

The model uses an empirical light response function of net assimilation An to combine the effects of light and CO_2 as limiting factors:

$$An = (Am + Rd) \left(1 - \exp\left(-\frac{\epsilon Ia}{Am + Rd}\right) \right) - Rd. \quad (1)$$

Am is the asymptotic value of the light response curve of photosynthesis, Rd is the dark respiration, ϵ is the initial light use efficiency, and Ia is the absorbed photosynthetically active radiation (aPAR). At very low light intensity, this asymptotic exponential becomes approximately:

$$An = \epsilon Ia - Rd, \quad (2)$$

reflecting that the photosynthetic rate is linearly related to the amount of aPAR at very low light intensity and nonlimiting CO_2 conditions.

When light is not limiting, Am is limited by a maximum photosynthetic rate $Ammax$ through another asymptotic exponential:

$$Am = Ammax \left(1 - \exp\left(\frac{-gm(Ci - \Gamma)}{Ammax}\right) \right), \quad (3)$$

where gm is the mesophyll conductance, Ci the intercellular CO_2 concentration and Γ the CO_2 compensation point. At low CO_2 concentrations, this equation is approximately equivalent to:

$$Am = gm(Ci - \Gamma), \quad (4)$$

stating that photosynthesis is linearly related to CO_2 concentration when CO_2 is limiting. In Goudriaan's model, this relation defines the mesophyll conductance gm as the initial slope of the A-Ci curve. As such, for C3 plants, gm can be related to $Vcmax$, the maximum catalytic capacity of Rubisco in Farquhar's formalism (see Farquhar, 1980, eq. 42):

$$gm = \frac{dA}{dCi} (Ci = \Gamma) = \frac{Vcmax}{\Gamma + Kc \left(1 + \frac{O_2}{K_o} \right)}, \quad (5)$$

where Kc and K_o are the Michaelis-Menten coefficients for CO_2 and O_2 respectively and O_2 is the oxygen concentration.

We used this relation to calculate gm using $Vcmax$ values given by Kattge et al. (2009) for all tree PFTs.

For C4 plants (with $\Gamma = 0$), following Collatz et al. (1992), $\frac{dA}{dCi} = k$ at low Ci so that $gm = k$ with k a constant per vegetation type, here only C4 grasses. For crops, we used the values of Canal et al. (2014).

According to Jacobs (1994), $Ammax$ is related to the ability of plants to allocate the products of the Calvin cycle and to regenerate ribulose 1,5-biphosphate and can be directly related to the maximum catalytic capacity of Rubisco $Vcmax$:

$$Ammax = l Vcmax, \quad (6)$$

with $l = 0.5$ for C3 plants (from Collatz et al., 1991, eq. A7) and $l = 1$ for C4 plants (from Collatz et al., 1992, eq. 5). We used this relation with $Vcmax$ values from Kattge et al. (2009) for all PFTs except one: for evergreen tropical trees, we used Domingues, Martinelli, and Ehleringer, (2007) observed value for tropical Amazonian sites (see Table 2).

Table 2
ISBA Parameter Values in the bgc5 and bgc6 Version

Vegetation type	<i>gm</i> (mm/s)		<i>A_{max}</i> (mg/m ² /s)		<i>N_m</i> (mg/g)		<i>SLA</i> (m ² /kg)	
	bgc5	bgc6	bgc5	bgc6	bgc5	bgc6	bgc5	bgc6
Temperate broadleaf cold-deciduous	3	1.8	2.2	1.3	20	21.3	12.2	15.4
Boreal needleleaf evergreen	2	1.9	2.2	1.4	28	12.1	13.3	5
Tropical broadleaf evergreen	1	1.2	2.2	0.5	25	17	14.6	8.3
C3 crops	1	1.8	2.2	2.2	13	13	14.8	14.8
C4 crops	9	9.8	1.7	1.7	19	19	10.3	10.3
Irrigated crops	9	9.8	1.7	1.7	19	19	10.3	10.3
C3 grass	1	1	2.2	1.7	13	13	14	14
C4 grass	6	6	1.7	1.7	13	13	5.7	5.7
wetlands	1	1	2.2	1.7	13	13	14	14
Tropical broadleaf dry-deciduous	3	1.2	2.2	0.9	20	21.3	12.2	15.4
Temperate broadleaf evergreen	3	1.9	2.2	1.3	20	16.9	12.2	8.3
Temperate needleleaf evergreen	2	1.9	2.2	1.4	28	12.1	13.3	5
Boreal broadleaf cold-deciduous	3	1.8	2.2	1.3	20	21.3	12.2	15.4
Boreal needleleaf cold-deciduous	2	1.2	2.2	0.9	28	19.4	13.3	10.1
Boreal grass	1	1	2.2	1.7	13	13	14	14
Deciduous shrub	3	1.6	2.2	1.2	20	21.5	12.2	15.4

Note. *gm*, unstressed mesophyll conductance (m/s); *A_{max}*, the maximum photosynthetic rate (10⁻⁶ kg_CO₂/m²/s); *N_m*, leaf nitrogen content per dry mass (mg_N/g_dry_matter); *SLA*, specific leaf area (m²/kgC). *N_m* and *SLA* are given for a 288-ppmv CO₂ level.

The temperature dependency of mesophyll conductance is given by an Arrhenius function, while standard Q10 temperature response functions determine CO₂ compensation point, maximum photosynthetic rate, and hence photosynthesis and respiration.

An important parameter in ISBA photosynthesis is the ratio of intercellular to atmospheric CO₂, *C_i/C_a*. This ratio is affected by the leaf-to-air vapor pressure deficit from a maximum value at zero deficit to a minimum value for which stomatal closure happens (Jacobs, 1994). Stomatal conductance is finally deduced from the assimilation rate taking into account cuticular conductance and diffusion competition between H₂O and CO₂ within the stomatal opening (see Jacobs, 1994). Hence, leaf-to-air vapor pressure deficit affects intercellular CO₂ and, through photosynthesis, stomatal conductance. Soil water stress affects the mesophyll conductance (see Joetzjer et al., 2015) and, through photosynthesis, stomatal conductance.

ISBA_bgc5 used Goudriaan's (1986) original 3-point Gaussian solution of the radiative transfer through canopy. In ISBA_bgc6, this was replaced by a 10-layer canopy radiative transfer scheme including direct and diffuse radiation (Carrer et al., 2013). Photosynthesis is calculated for each of the 10 layers and summed to calculate canopy level assimilation.

2.2. Respiration

Joetzjer et al. (2015) showed that ISBA_bgc5 greatly overestimated leaf respiration in the Amazon Forest. Following Van Heemst (1986), leaf dark respiration integrated over the canopy was originally parameterized as a fraction of *A_m* (Gibelin et al., 2006), the photosynthetic rate at high light intensities (equation 1):

$$R_{\text{leaf}} = \frac{A_m}{9} LAI. \quad (7)$$

A_m being constant throughout the canopy, this leads to identical respiration from the top to the bottom of the canopy, and a negative carbon balance of the bottom canopy leaves because of light extinction. Observations show that leaf respiration is positively correlated to area-based leaf nitrogen content, which in turn is driven by light availability. We therefore follow Bonan et al. (2012), who proposed to scale leaf to canopy respiration by using a vertical exponential profile of leaf nitrogen:

$$R_{\text{leaf}} = \frac{Am}{9} \exp(-k_n LAI), \quad (8)$$

where k_n is the within-canopy profile of photosynthetic capacity set to 0.2 according to Mercado et al. (2009) and Bonan et al. (2011). This parametrization greatly reduces the leaf dark respiration of the canopy compared to the original one. We chose to keep the same k_n value for all tree species for simplicity sake, but this should be tested and revised in future versions.

ISBA_bgc5 (Gibelin et al., 2008) did not allow for sapwood respiration. As described in Joetzjer et al. (2015), we added a representation of sapwood respiration based on Kucharik et al. (2000):

$$R_{\text{wood}} = B_{\text{wood}} \lambda_{\text{sap}} \beta_{\text{wood}} f(T), \quad (9)$$

with B_{wood} the woody biomass, λ_{sap} the estimated sapwood fraction based on a theoretical sap velocity, the maximum transpiration rate and the tree height. $\beta_{\text{wood}} = 0.0125$ year is the maintenance respiration coefficient at 288 K and $f(T)$ is given by Lloyd and Taylor (1994) version of the Arrhenius temperature function:

$$f(T) = \exp\left(E_0 \left(\frac{1}{288} - \frac{1}{T}\right)\right), \quad (10)$$

with $E_0 = 3,500^\circ\text{K}$, the temperature sensitivity, and T (in K), the vegetation temperature, calculated as the weighted average of vegetation and soil surface temperature in ISBA (Noilhan & Planton, 1989).

This formulation was also adopted for the respiration of twigs and fine roots, $R_{\text{twigs-root}}$, using a maintenance respiration coefficient $\beta_{\text{twigs-roots}}$ of 1.25 year (Joetzjer et al., 2015).

$$R_{\text{twigs-root}} = B_{\text{twigs-root}} \beta_{\text{twigs-root}} f(T). \quad (11)$$

2.3. Vegetation Carbon Pools

Vegetation in ISBA is represented by a maximum of six reservoirs of biomass: leaves, stem/twigs, wood, fine and coarse roots, and a small storage pool (Gibelin et al., 2008) that can be seen as a nonstructural carbohydrate pool. In the case of grasses and crops, wood and the coarse root reservoirs are not represented. Leaf biomass is based on the carbon assimilated by photosynthesis and decreased by turnover, respiration, and allocation to the other pools (see Gibelin et al., 2006, annex B). Leaf phenology results directly from the daily carbon balance of the leaves. Leaf area index (LAI) is diagnosed from leaf biomass and specific LAI, which varies as a function of leaf nitrogen concentration and PFT (see section 2.5). To allow for leaf growth after dormancy, there is an imposed minimum leaf biomass. Mortality is represented as turnover with a PFT-dependent turnover time for the wood and root carbon pools. It depends on climate conditions for leaves and twigs. The evolution of the different vegetation carbon pools is calculated once a day, while photosynthesis and respiration are calculated every 15 min to an hour (depending on the forcing data).

2.4. Litter and Soil Organic Matter

The litter and soil organic matter module in ISBA is based on the soil carbon part of the CENTURY model (Parton et al., 1988). The four litter and three soil carbon pools are defined based on their presumed chemical composition, their location aboveground or belowground, and potential decomposition rates (or turnover times). The litter pools (metabolic and structural, above and belowground) are supplied by the fluxes of dead biomass from each biomass reservoir (turnover) as described in Gibelin et al. (2008). The decomposition process is represented by organic matter cascading from pool to pool with different turnover times, releasing CO_2 at each step. The three soil organic matter reservoirs (active, slow, and passive) are characterized by their resistance to decomposition with turnover times spanning from a few months for the active pool to 240 years for the passive pool (Gibelin et al., 2008). The rate of decomposition of organic matter is determined mainly by soil moisture and temperature using a Q10 dependency following the formulation of Krinner et al. (2005). The decomposition rate also depends on the lignin fraction and the soil texture following Parton et al. (1988).

2.5. Dependence of SLA on N Content and Link With Atmospheric CO₂-Downregulation

ISBA does not represent N and P cycles, and nutrient limitation effects on photosynthesis and plant growth are not represented explicitly. The model however has an empirically based reduction of leaf nitrogen concentration per unit mass with increasing CO₂ (Calvet et al., 2008) as proposed by Yin (2002) from a meta-analysis of CO₂ enrichment experiments. The model also linearly relates SLA to leaf nitrogen concentration per unit mass (Gibelin et al., 2006). As a result, specific leaf area decreases with increasing CO₂ concentration, which limits leaves growth and indirectly limits assimilation of atmospheric CO₂. This trait plasticity behavior has indeed been reported for a variety of species (Ainsworth & Long, 2005; De Kauwe et al., 2014; Ishizaki et al., 2003; Medlyn et al., 2015; Yin, 2002) but with different strengths and explained by more complex processes than those assumed in ISBA's simple empirical representation.

Nitrogen deficiency, regardless of CO₂ increase, not only affects SLA and other traits but also directly affects photosynthesis (see for instance Norby et al., 2010). This effect is not represented in ISBA's physiological module. In the absence of a full representation of nutrient cycles, we chose to use an ad hoc representation of downregulation similar to Arora et al. (2009). Leaf level gross photosynthesis is multiplied by ζ , a factor equal to 1 at preindustrial concentration (below CO_{2ref} = 288 ppmv) and decreasing with increasing CO₂ concentration:

$$\zeta(\text{CO}_2) = \frac{1 + 0.52 \ln \frac{\text{CO}_2}{\text{CO}_{2\text{ref}}}}{1 + 0.9 \ln \frac{\text{CO}_2}{\text{CO}_{2\text{ref}}}}. \quad (12)$$

For the time period simulated here (see section 3), ζ varies from 1 in 1870 to 0.91 in 2010.

2.6. Plant Functional Types

ISBA_bgc5 used nine PFTs (three tree types, three grass types, and three crop types) and three land covers (bare soil, rock, and permanent snow and ice) derived from the ECOCLIMAP vegetation and soil database (Masson et al., 2003). The tree types (broadleaf deciduous, needleleaf evergreen, and tropical broadleaf evergreen) did not allow for a correct representation of plant types covering large or important areas like the deciduous needleleaf forests of Eastern Siberia, the tropical deciduous broadleaf forests of subtropical Africa, or the dry broadleaf evergreen forests in Mediterranean climates. We therefore added five tree types distinguishing boreal and temperate types and one deciduous shrub type using the updated ECOCLIMAPII database (Faroux et al., 2013). Similarly, we added an arctic grass PFT. The geographical distribution of boreal, temperate, and tropical tree types is based on LPJ bioclimatic limits (Table 2 in Sitch et al., 2003). Arctic grasses were defined using information present in the original ECOCLIMAP database. Shrubs were defined as deciduous trees less than 2 m high. The resulting PFT distribution for year 2000 is given in Figure 2 with the dominant vegetation type. The wetland and irrigated crop vegetation types are currently treated by the model as simply grass and crops.

Vegetation height and vegetation and soil albedos are prescribed for all the surface types subgrid patches based on a mean annual cycle at a 10-day time step. Vegetation and bare soil albedos in ECOCLIMAP are derived from satellite observations (Carrer et al., 2014). The rooting depth is specified for each vegetation type according to Canadell et al. (1996). It ranges from 0.5 to 1.5 m for tundra and temperate grassland and from 2 to 8 m for forest. Carbon cycling, energy, and water balance in vegetation and soils are computed separately for all the coexisting PFTs and cover types present in the grid cell. Land cover changes were not represented in ISBA_bgc5, ECOCLIMAP being representative of the land cover of the 1990s.

2.7. Land Cover Change

ISBA_bgc6 does not represent natural vegetation dynamics, defined as the change in geographical distribution of natural PFTs in response to climatic changes. However, contrary to ISBA_bgc5 that used a fixed geographical distribution of anthropogenic land cover (crop and pasture), ISBA_bgc6 represents net land cover changes. They are resolved at a yearly time step although the procedure might be used at a higher frequency (monthly or daily). Net land cover changes (see Figure 1 in Stocker et al., 2014 for a definition of net changes) are derived from the Land-Use Harmonized data sets (Hurtt et al., 2011) version 2.0h (LUH2.0h, <http://luh.umd.edu/data.shtml>) using the ECOCLIMAP land cover distribution of the 1990s described in section 2. We project LUH2.0h on the ISBA PFTs as follows:

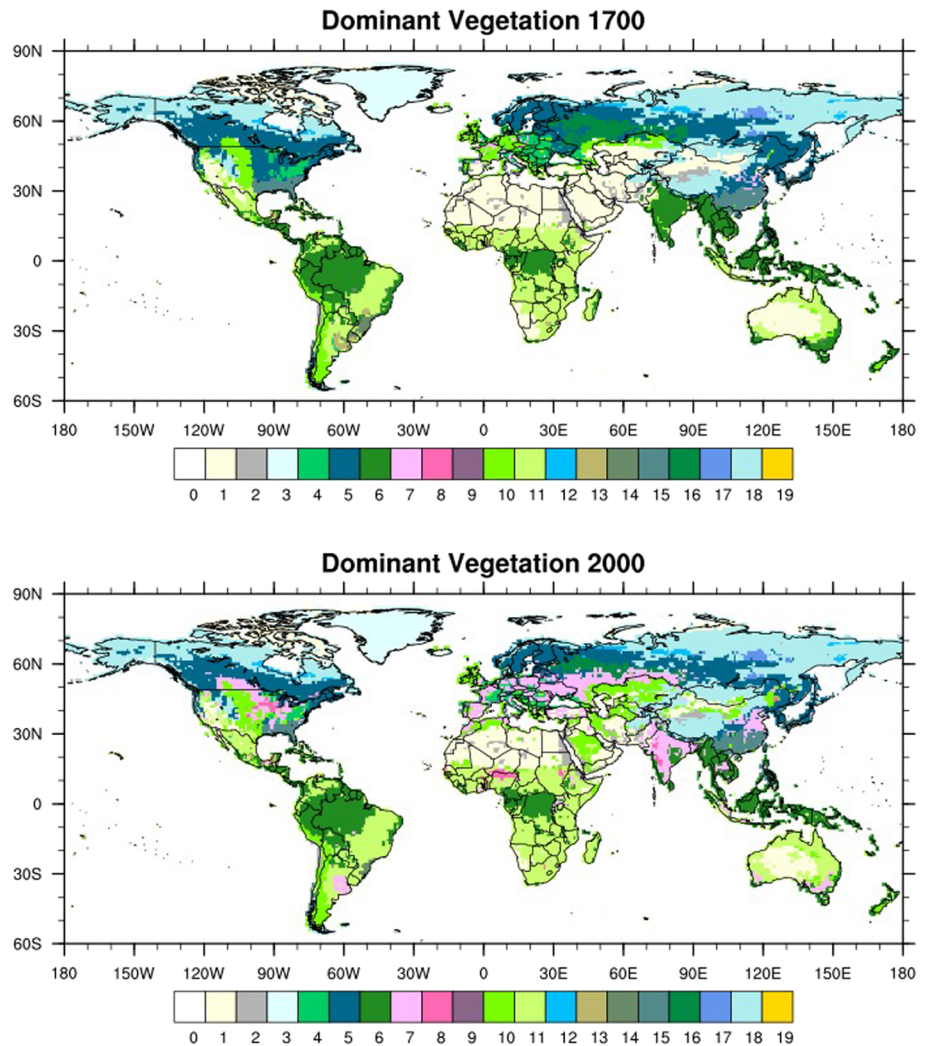


Figure 2. Distribution of dominant vegetation type in years 1700 and 2000 resulting from the combination of ECOCLIMAP and LUH2.0h. (1) desert, (2) rock, (3) permanent snow and ice, (4) temperate broadleaf deciduous trees, (5) boreal needleleaf evergreen trees, (6) tropical broadleaf evergreen trees, (7) C3 crops, (8) C4 crops, (9) irrigated C4 crops, (10) C3 grass, (11) C4 grass, (12) wetland, (13) tropical broadleaf evergreen trees, (14) temperate broadleaf evergreen trees, (15) temperate needleleaf evergreen trees, (16) boreal broadleaf deciduous, (17) boreal needleleaf deciduous, (18) boreal grass, and (19) deciduous shrubs.

- LUH2.0h C3 and C4 crops are used directly as ISBA C3 and C4 crop PFTs.
- LUH2.0h anthropogenic pasture and rangeland are combined and used to compute the fraction of anthropogenic grasslands and shrubs for ISBA. The partition between shrubs, C3, C4, and boreal grasslands in ISBA is inferred from the partition of ECOCLIMAP in the considered grid cell. If ECOCLIMAP does not include any of these PFTs in the considered grid cell, the fraction of combined pasture and rangeland from LUH2.0h is assumed to be C3 grass.
- The other PFTs, including forested areas, are then scaled using the remaining fraction of land as given by LUH2.0h and the partition between PFTs from ECOCLIMAP.

During these steps, we ensure that the fraction of rock and permanent ice as given by ECOCLIMAP remains unchanged. To do that and to conserve as much as possible anthropogenic land cover changes given by LUH2.0h, we do not conserve the partition between the other vegetation types of LUH2.0h especially the forested areas. Before running this procedure, LUH2.0h is interpolated on ISBA spatial grid using a conservative interpolation. To illustrate the approach, we show the resulting dominant vegetation types in Figure 2 for years 1700 and 2000, where we clearly see the increase in cropland over the midlatitudes.

Table 3
Fraction of Aboveground Biomass Routed Toward the Three Anthropogenic Carbon Pools Following Land Cover Change

Vegetation type	Veg → atm (–)	Veg → Anth ^{10y} (–)	Veg → Anth ^{40y} (–)
Temperate broadleaf cold-deciduous	0.597	0.299	0.104
Boreal needleleaf evergreen	0.597	0.299	0.104
Tropical broadleaf evergreen	0.597	0.299	0.104
C3 crops	0.597	0.403	0.000
C4 crops	0.597	0.403	0.000
Irrigated crops	0.597	0.403	0.000
C3 grass	0.597	0.403	0.000
C4 grass	0.597	0.403	0.000
Wetlands	0.597	0.403	0.000
Tropical broadleaf dry-deciduous	0.597	0.299	0.104
Temperate broadleaf evergreen	0.597	0.299	0.104
Temperate needleleaf evergreen	0.597	0.299	0.104
Boreal broadleaf cold-deciduous	0.597	0.299	0.104
Boreal needleleaf cold-deciduous	0.597	0.299	0.104
Boreal grass	0.597	0.299	0.104
Deciduous shrub	0.597	0.403	0.000

When land cover changes from 1 year to the next, ISBA handles water and carbon conservation for all the co-existing PFTs and cover types present in the grid cell. For water, changes in land water storage due to land cover changes including different soil depth or interception of snow and rain over vegetation when forest is replaced by grassland for instance are routed toward runoff using a water buffer with a characteristic time of 1 year. For carbon, a fraction of the aboveground biomass is routed toward three anthropogenic carbon pools with annual, decadal, and multidecadal turnover times ($fLUC_{Veg \rightarrow Anth^\tau}$). These anthropogenic pools represent the use of harvested biomass as grain/forage, paper fabrication, and construction. The fraction of biomass routed toward these pools is given in Table 3. The aging processes in the decadal and multidecadal anthropogenic carbon pools are represented as first-order systems with an exponential decay time of 10 and 40 years. The decaying fraction is released back to the atmosphere ($fLUC_{Anth^\tau \rightarrow atm}$). For the sake of simplicity, and because the land cover changes are applied with a 1-year time step, we assume that all the cleared aboveground biomass routed toward the annual anthropogenic carbon pool go directly to the atmosphere ($fLUC_{Veg \rightarrow atm}$). The remaining biomass, the belowground biomass, is routed toward the metabolic belowground litter pool ($fLUC_{Veg \rightarrow litter}$).

The carbon flux from the anthropogenic pool to the atmosphere is defined as the sum of the carbon fluxes of the 10- and 40-year anthropogenic carbon buffer, that is, $fLUC_{Anth \rightarrow atm} = fLUC_{Anth^{10y} \rightarrow atm} + fLUC_{Anth^{40y} \rightarrow atm}$.

Finally, when a new PFT is created within an ISBA grid cell, a minimum LAI and biomass is automatically allocated to this new vegetation. We call this small annual flux of carbon the regrowth flux $fLUC_{atm \rightarrow Veg}$. In this case, and because of the soil column paradigm used in ISBA (separate soil columns for each surface type), the litter and soil carbon content for this newly created PFT is deduced from the total grid cell litter and soil carbon balance.

2.8. Fire

The fire carbon module implemented in ISBA derives from GlobFIRM (Thonicke et al., 2001). It represents natural wildfires over forest and grassland areas. The GlobFIRM fire fraction calculation is adapted to a daily time step using the same methodology as Krinner et al. (2005). It has been recalibrated using Météo-France fire occurrence measurements over the 2000s. It is set to zero when the carbon content of the surface litter is below 200 gC/m² and when soil temperature is lower than 0°C or when the soil is frozen. It is also set to zero when more than 20% of the grid cell is covered by croplands. Agricultural fires are not negligible (8–11% of all fire occurrences in 2001–2003 according to Koronzi et al. (2006)) but are largely related to human practice (see for instance Lin et al., 2014), and we only represent natural fires. The fire fraction ϕ_{fire} governs all the other fire-related process.

Table 4
PFT-Dependent Fire Parameters: Fire Resistance and Emissions Factors for Carbon Dioxide (CO₂) and Black Carbon (BC)

Vegetation type	$\rho^{\text{pft}} (-)$	$\epsilon_{\text{CO}_2}^{\text{pft}} \left(\text{kg}_{\text{CO}_2} / \text{kg}_{\text{DryMatter}} \right)$	$\epsilon_{\text{BC}}^{\text{pft}} \left(\text{g}_{\text{BC}} / \text{kg}_{\text{DryMatter}} \right)$
Temperate broadleaf cold-deciduous	0.62	1.572	0.56
Boreal needleleaf evergreen	0.62	1.572	0.56
Tropical broadleaf evergreen	0.90	1.636	0.52
C3 crops	1.	1.646	0.46
C4 crops	1.	1.646	0.46
Irrigated crops	1.	1.646	0.46
C3 grass	0.	1.646	0.46
C4 grass	0.	1.646	0.46
wetlands	0.5	1.703	0.57
Tropical broadleaf dry-deciduous	0.90	1.636	0.52
Temperate broadleaf evergreen	0.62	1.572	0.56
Temperate needleleaf evergreen	0.62	1.572	0.56
Boreal broadleaf cold-deciduous	0.62	1.572	0.56
Boreal needleleaf cold-deciduous	0.62	1.572	0.56
Boreal grass	0.05	1.646	0.46
Deciduous shrub	0.60	1.572	0.56

Fire consumes living biomass pending on the fire resistance of each PFT (ρ^{pft} , see Table 4) and of the water-to-biomass fraction in each compartment (i) of the plants i (see Table 5). i is consistent with estimates used in other models (see for instance INFERNO of Mangeon et al., 2016).

$$B_{\text{disturbed}}^{\text{pft}} = \sum_{i=1}^6 (1 - \rho^{\text{pft}}) \times B_i^{\text{pft}} \times i \times \phi_{\text{fire}}, \quad (13)$$

where $B_{\text{disturbed}}^{\text{pft}}$ is the total amount of living biomass impacted by fire.

$B_{\text{disturbed}}^{\text{pft}}$ is used to compute the fire-induced emissions of carbon dioxide (CO₂) and black carbon (BC) using the Akagi et al. (2011) emission factors for these two chemical species and for a given PFT ($\epsilon_{\text{CO}_2}^{\text{pft}}$ and $\epsilon_{\text{BC}}^{\text{pft}}$; see Table 4).

$$f_{\text{Veg} \rightarrow \text{CO}_2} = \sum_{\text{pft}} \epsilon_{\text{CO}_2}^{\text{pft}} B_{\text{disturbed}}^{\text{pft}}, \quad (14)$$

$$f_{\text{Veg} \rightarrow \text{BC}} = \sum_{\text{pft}} \epsilon_{\text{BC}}^{\text{pft}} B_{\text{disturbed}}^{\text{pft}}. \quad (15)$$

The remaining fraction of the living biomass is added to the surface refractory litter (i.e., structural).

$$f_{\text{Veg} \rightarrow \text{cLitter}_{\text{surf,structural}}} = \sum_{\text{pft}} B^{\text{pft}} - B_{\text{disturbed}}^{\text{pft}}. \quad (16)$$

In this fire module, only the surface litter is impacted by fire. All the young labile surface litters (i.e., metabolic) are consumed by fire and converted in CO₂ and BC using (Akagi et al., 2011) emission factors. The old refractory surface litter is also impacted, but its consumption by fire depends on its content in lignin ($\text{lignin}^{\text{pft}}$). As a consequence, the fire emission for CO₂ or BC is computed as follows:

$$f_{\text{cLitter}_{\text{surf}} \rightarrow X} = \sum_{\text{pft}} \epsilon_X^{\text{pft}} (\text{cLitter}_{\text{surf,metabolic}} + \text{lignin}^{\text{pft}} \times \text{cLitter}_{\text{surf,structural}}) \times \phi_{\text{fire}}, \quad (17)$$

where X is CO₂ and BC.

2.9. Carbon Leaching

The movement of water in and above the soil transports carbon stored in the soil. Part of the soil carbon is dissolved in the water, and a fraction of this DOC leaves the soil laterally to enter the aquatic continuum,

Table 5
Sensitivity of Plant Compartment to Fire Disturbance

Plant's compartments	Leaf (–)	Stem (–)	Wood (–)	Root (–)
<i>i</i>	0.85	0.80	0.3	0.05

be transported by the rivers and ultimately released to the ocean. Total anthropogenic and natural carbon export from the soils to the inland waters is estimated to be around 1.9 PgC/year for the years 2000–2010, among which roughly half reaches estuaries (Regnier et al., 2013). In between, DOC may be mineralized, buried in sediments, and remobilized. The flux of carbon leached out of the soil is much smaller than photosynthesis (around 110 PgC/year) or autotrophic and heterotrophic respiration (around 50–55 Pg/year) but is a nonnegligible carbon input to the global ocean. It is also essential for accurately representing the patterns of ocean C flux (Resplandy et al., 2018). Therefore, it needs to be represented in a model that is used as the land surface component of an ESM.

As mentioned in section 2.4, the soil carbon module in ISBA is based on the CENTURY model. In this framework, we chose a simple approach to represent this leaching of carbon from the soil column and the input of carbon to the ocean. We assume that a fraction of organic matter is dissolved in water at each step of the decomposition cascade so that the mobilization of DOC is controlled by the same environmental factors as decomposition in the model: soil temperature and moisture content (see section 2.4). But we consider that it only happens in the saturated fraction of a grid cell or, in the case of superficial litter, the fraction that is inundated. This approach is reasonable since bacterial and fungal decomposers are responsible for most of the organic matter decomposition (Wetterstedt, 2010) and they indeed rely on water to access their substrate (Marshner & Kalbitz, 2003).

During the decomposition of each carbon pool (litter and soil carbon), the flux of carbon dissolved in water $fDOC$ ($gCm^{-2}s^{-1}$) is calculated as

$$fDOC_{agi} = \frac{1}{\tau_i} f_1(T_1) f_2(w_1) mobil \max(fsat, fflood) C_{agi}, \quad (18)$$

for the aboveground reservoirs C_{agi} and

$$fDOC_{bgj} = \frac{1}{\tau_j} f_1(T_2) f_2(w_2) mobil fsat C_{bgj}, \quad (19)$$

for the belowground reservoirs C_{bgj} . T_1 and w_1 are the soil surface temperature and moisture content, T_2 and w_2 are the temperature and moisture content averaged over the first meter of soil. f_1 and f_2 are the environmental functions (see eqs. 1–5 of Morel et al., 2019) and τ_i and τ_j are the turnover times of the different litter and carbon reservoirs. $mobil = 0.005$ is the maximum fraction of litter or soil carbon mobilized and dissolved. This empirical parameter is inspired from modeling work by Langerwisch et al. (2016) and Imler (1982). Since we chose not to represent the processes happening in the rivers and lakes once the SOC has left the soil column, we use a value of $mobil$ that ensures the right order of magnitude of DOC reaching the ocean. $fsat$ is the fraction of the grid cell where soil is saturated and $fflood$ the fraction of the grid cell inundated. A complete description of the hydrological cycle in ISBA is given in Decharme et al. (2019).

The total flux of DOC leaching from the soil, $fDOC_{tot}(t) = \sum_i fDOC_{agi} + \sum_j fDOC_{bgj}$, is then routed toward the closest river channel. Within the river, the DOC content (DOC in gC) is handled by CTRIP as

$$\frac{\partial DOC}{\partial t} = A fDOC_{tot} - \frac{v(t)}{L} DOC(t), \quad (20)$$

where A is the area of the considered ISBA grid cell, $v(t)$ and L represent the velocity of the river flow (in m/s) and the length of the river in the grid cell. As mentioned before, equation 20 does not include biogeochemical or sedimentary processes that would modify DOC concentration during its course in the river channel. CTRIP does not include other carbon-related chemical species such as dissolved inorganic carbon which would enable the computation of air-water carbon exchange.

3. Model Configuration and Observation Used

3.1. Model configuration

To document the impact of the changes between ISBA_bgc5 and ISBA_bgc6 on the simulated carbon cycle, we performed two paired model simulations (1860–2016) on a $1^\circ \times 1^\circ$ global terrestrial grid driven by the same climate data and soil boundary conditions. ISBA_bgc6 was forced by changing land cover from LUH2.0h as described in the previous section. ISBA_bgc5 ran with constant vegetation cover given by ECOCLIMAP representative of the land cover in the 1990s. The model simulations went through an initial 350-year spin-up procedure where soil carbon and vegetation biomass were allowed to reach an equilibrium state representative of 1860. During this initial spin-up period, the soil biogeochemistry module was subjected to a numerical acceleration procedure to reduce the computational burden. Litter input from vegetation turnover and decomposition from litter pools and soil carbon was assumed to occur at 50 times the normal rate during the first 150 years. During the next 50 years, the acceleration rate was linearly reduced to 1. The last 150 years ran without acceleration. Vegetation woody biomass underwent a similar numerical acceleration procedure during the first 30 years with an acceleration rate of 5. Consequently, the spin-up period for soil carbon is about 7,500 years and 150 years for vegetation biomass. This method similar to Kucharik et al.'s (2000) was successfully tested at point scale in different climate conditions.

The historical climate forcing used is the CRU-NCEP v7 data set from Viovy (2018) covering 1901–2016, with global atmospheric CO₂ concentration from Meinshausen et al. (2017). The initial spin-up period assumed a preindustrial CO₂ concentration of 286.4 ppmv and was driven by recycling years 1901–1920 from the climate forcing. Years 1860 to 1900 were simulated using the same 1901–1920 period twice but with the actual observed CO₂ concentration. The CRU-NCEP product has a 0.5° spatial resolution and a 6-hr temporal resolution. ISBA uses a 900-s time step and interpolates in time the climate forcing. To limit computing time, we degraded the original spatial resolution to 1° . To focus our comparison on the representation of the carbon cycle, we used the new physics of the model described in Decharme et al. (2019) in both versions of the model.

The soil textural properties and the soil carbon content affecting the physical soil properties (Decharme et al., 2016) are given by the Harmonized World Soil Database (HWSD; <http://www.fao.org/soils-portal/soil-survey/soil-maps-and-databases/harmonized-world-soil-database-v12/en>). The topographic information comes from the 30-arcsecond resolution GTOPO30 data.

3.2. Evaluation data

We use an ensemble of available global observations derived from remotely sensed data, in situ data, or combinations of remotely sensed, in situ eco-physiological data, census data, and climate reanalysis to evaluate the model simulated carbon fluxes and pools:

- The FluxComV1 data sets for gross primary productivity (GPP) and terrestrial ecosystem respiration. These products come from the FLUXCOM project (Jung et al., 2016, 2017; Tramontana et al., 2016). They combine remote sensing and meteorological data to upscale the global network of eddy covariance FLUXNET tower data (Jung et al., 2009). They have a daily time step, a 0.5° spatial resolution and cover 1980–2014 (<http://www.fluxcom.org>).
- The satellite derived GPP and net primary productivity (NPP) product from the Numerical Terradynamic Simulation Group: MODIS17A3 (Zhao et al., 2005). This product derived from the Moderate Resolution Imaging Spectroradiometer (MODIS) on board the U.S. National Aeronautics and Space Administration (NASA) Earth Observation System (EOS) satellite Terra has a yearly time step and a 1-km spatial resolution to compare with model results (NASA LP DAAC, 2017). It covers years 2000–2013 (<https://modis.gsfc.nasa.gov/data/dataproduct/mod17.php>).
- The Harvested Area and Yield for 175 crops data set described in Monfreda, Ramankutty, and Foley (2008) to compare crop NPP. This land use data set combines national, state, and county level census statistics with a global data set of croplands, on a 5-min \times 5-min spatial grid and is representative of the years 2000 (<http://www.earthstat.org>).
- For heterotrophic respiration, we use the data set from Hashimoto et al. (2015) that combines in situ data from the Soil Respiration database (Bond-Lamberty et al., 2018) and global gridded climate data. It is

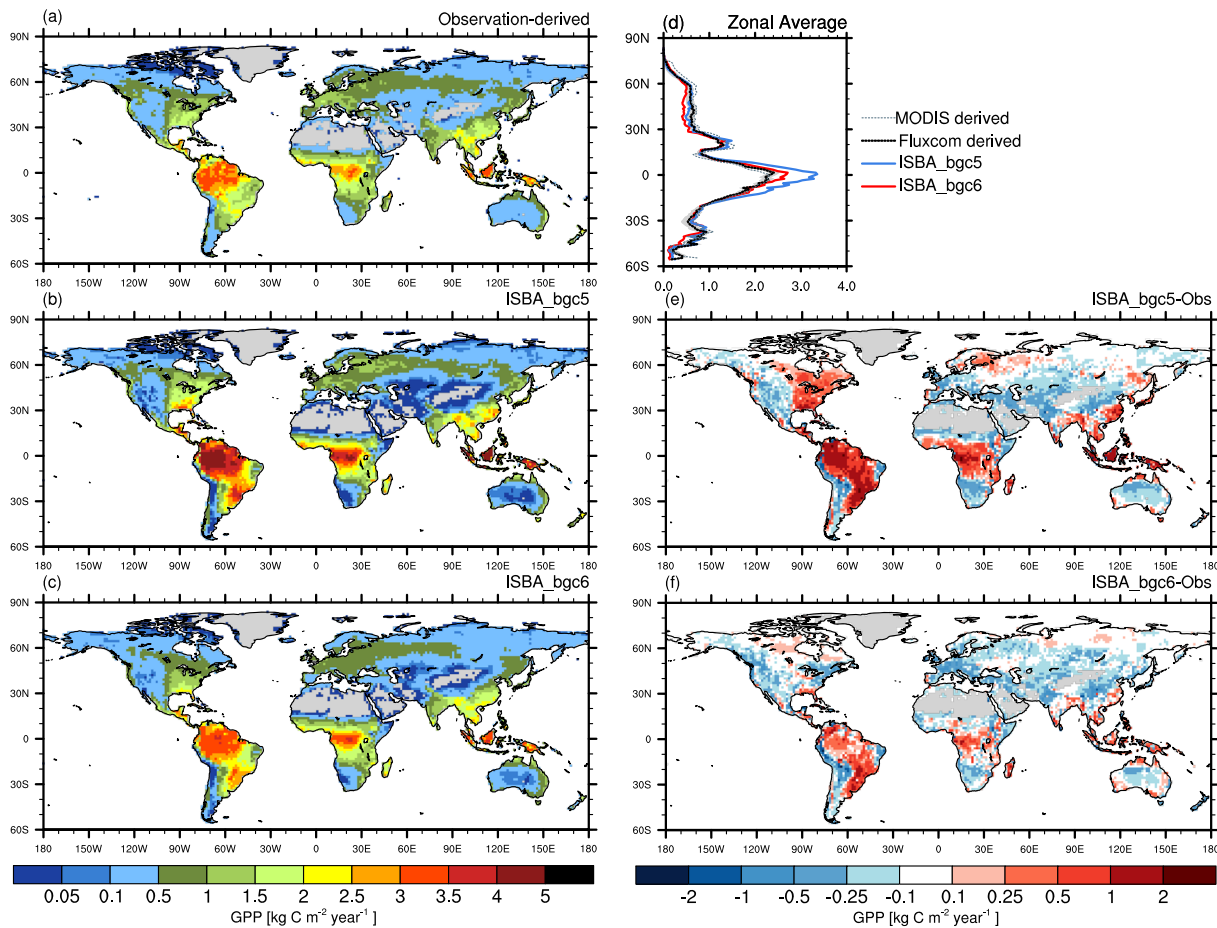


Figure 3. Gross primary productivity (GPP). (a) Mean of 12 FluxCom products, (b) simulated with ISBA_bgc5, (c) simulated with ISBA_bgc6, and (d) zonal average observation-derived and simulated GPP. The gray shading indicates the spread between the FluxCom products. (e) ISBA_bgc5 minus observation derived and (f) ISBA_bgc6 minus observation-derived.

based on data from 1965 to 2012 and has a 0.5° spatial resolution (<http://cse.ffpri.affrc.go.jp/shojih/data/index.html>).

- The simulated burned area is compared to the yearly maps at 1° resolution of burnt area derived from satellite data, census data, and vegetation by Mouillot and Field (2005). CO_2 emissions from fire come from the Global Fire Emissions Database, Version 4.1 (GEFD4, van der Werf et al., 2017; Randerson et al., 2017) (<https://www.globalfiredata.org/data.html>).
- The DOC originating from soil carbon leaching is compared to the global, spatially explicit, multielement, and multiform model of nutrient exports by rivers (NEWS2, <https://marine.rutgers.edu/globalnews/datasets.htm>) described in Mayorga et al. (2010). This product was calibrated at global scale using nutrient export observations at river mouths and allowed a spatially distributed comparison with our simulation results. The simulated riverine DOC flux to the ocean is also directly compared to river data from Dai et al. (2012).
- The aboveground biomass carbon (ABC) data set is derived from satellite-based passive microwave observations of the vegetation optical depth (Liu et al., 2015). The data set covers 1993–2012 at a yearly time step and a 0.25° spatial resolution (http://wald.anu.edu.au/data_services/data/global-above-ground-biomass-carbon-v1-0/). Additional regional data sets are Thurner et al. (2014) for the midlatitude to high latitude of the Northern Hemisphere and Saatchi et al. (2011) and Baccini et al. (2012) for the tropics (see Table S1 in the supporting information).
- Aboveground Litter Carbon comes from the “Global Database of Litterfall Mass and Litter Pool Carbon and Nutrients” (Holland et al., 2015). It includes site measurements of among others aboveground litter

Table 6
Global Carbon Fluxes and Pools Derived From Observations Described in Section 3 and Calculated by ISBA_bgc5 and ISBA_bgc6

	Observation derived	ISBA_bgc5			ISBA_bgc6		
	Total	Total	Bias	Spatial correlation	Total	Mean bias	Spatial correlation
GPP (1980–2014)	115 +/- 6.5	129	0.13	0.93	110	-0.03	0.93
NPP ^a (2000–2013)	44.6	39.9	-0.05	0.67	41.1	-0.04	0.81
		48.5			49.3		
Ra ^b (2000–2013)	53.4	76.1	0.25	0.89	56.5	0.04	0.89
		89.8			66.3		
Rh (1962–2012)	46.9	37.7	-0.08	0.74	37.2	-0.08	0.84
TER (1980–2014)	92.4 +/- 3.4	126	0.28	0.92	104	0.1	0.92
GPP-TER	22.6	3			6		
Fire C emissions (1997–2015)	2.14	-	-	-	2.71	0.004	0.41
DOC flux	0.18	-	-	-	0.13	-	-
fLCC ^c (2000–2009)	1.3 +/- 0.7				0.79		
Biomass		399	-	-	488	-	-
ABC	348	324	-0.17	0.70	438	0.75	0.79
Aboveground litter		295			157		
Belowground litter		115			123		
SoilC	1613	1611	0.16	0.54	1520	-0.45	0.56

Note. Total fluxes are in PgC/year and mean biases in kgC/m²/year.

^aThe MODIS NPP product contains missing data. The first line gives simulation results on the nonmissing data mask. The second line gives the total/average land values. ^bObservation-derived Ra is estimated using FluxCom GPP minus MODIS NPP for 2000–2013. ^cFlux from Land Cover Change (fLCC): Estimates from bookkeeping methods, see Table 5 from Le Quéré et al., 2018.

mass and litter carbon dating from 1827 to 1997 (https://daac.ornl.gov/VEGETATION/guides/Global_Litter_Carbon_Nutrients.html).

- Belowground organic carbon fraction comes from the Harmonized World Soil Database v1.2 (FAO/IIASA/ISRIC/ISSCAS/JRC, 2012). We derived the organic carbon mass using soil density data from the database (<http://webarchive.iiasa.ac.at/Research/LUC/External-World-soil-database/HTML/>).
- The LAI3g product derived from the third generation of the Normalized Difference Vegetation Index (NDVI3g) by the Global Inventory Modeling and Mapping Studies (GIMMS) group. The NDVI3g from the Advanced Very High Resolution Radiometer (AVHRR) sensors was released for the period 1981 to 2011 (Zhu et al., 2013). The original 15-day time resolution and 1/12° spatial resolution was averaged to a monthly time step and 1° spatial resolution. We compare the peak and minimum LAI computed as the maximum and minimum of the average seasonal cycle (https://daac.ornl.gov/VEGETATION/guides/Mean_Seasonal_LAI.html).

It is important to notice that these global data sets are observation derived but are not true observations and may have large uncertainties and biases. We use them as benchmark for large-scale evaluation, but the model was also evaluated at local scale with Fluxnet data (see Joetzjer et al., 2015).

4. Skill Assessment of Key Land Surface Variables Against Present-Day Observation

For each flux and pool, we present a comparison between observation-derived data and the results of ISBA_bgc5 and ISBA_bgc6 forced by the same atmospheric forcing, CRU-NCEPv7. The comparison is done for the period covered by the data, usually 1980–2010. We here mainly focus on the mean state. Interannual variability was studied by Bastos et al. (2018), who looked at the response of several models to the 2015 El Niño.

4.1. Carbon Fluxes

GPP is the primary driver of the carbon cycling in vegetation and soils as it is the input flux of the system in the model. We compare the geographical distribution of the annual mean-simulated GPP to the average of the 12 reconstruction products of the FluxCom project described in section 3 (Figures 3a–3c). The spread between these observation derived products is presented in the zonal mean (Figure 3d). Compared to these reconstructions, the simulated GPP is greatly improved in the ISBA_bgc6 version compared to the

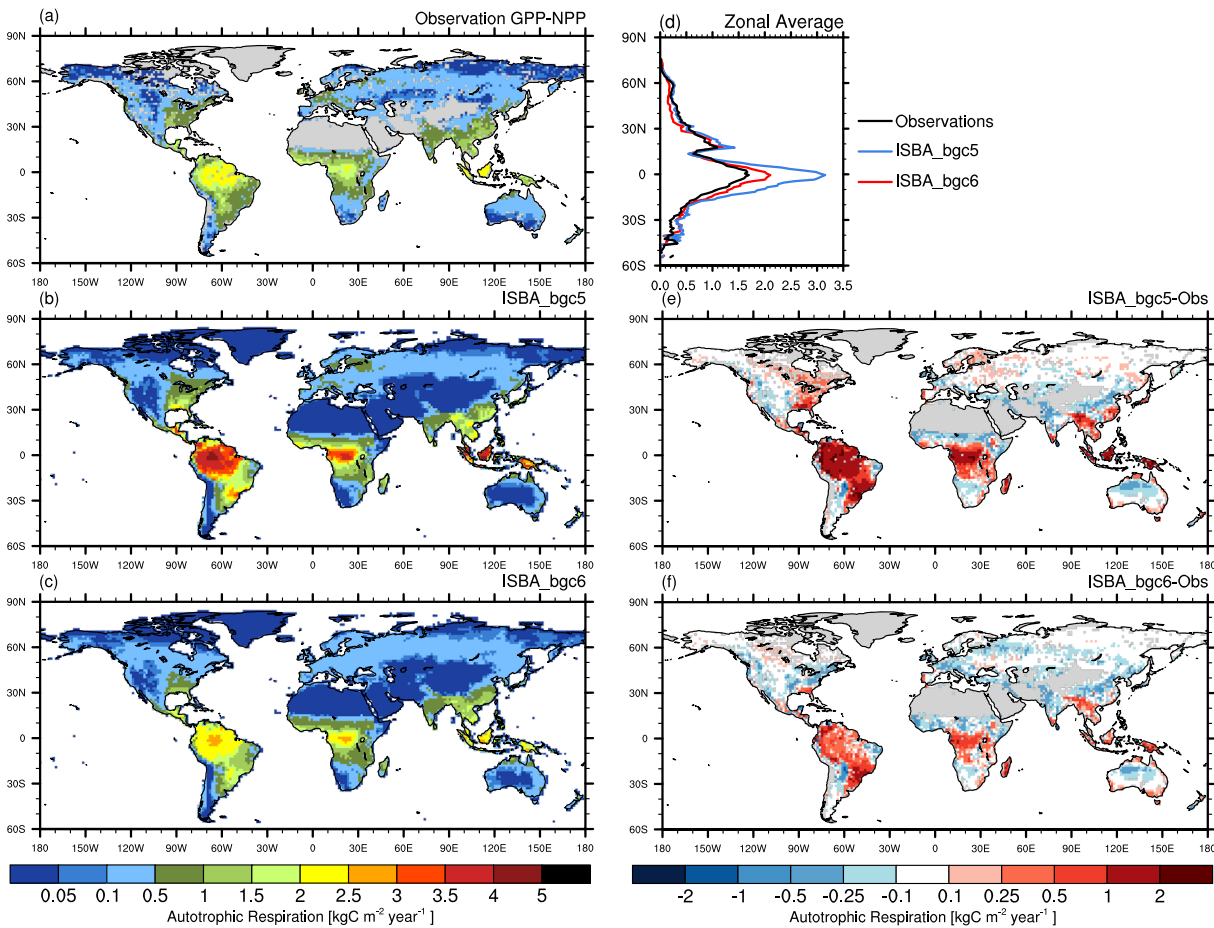


Figure 4. Autotrophic respiration (R_a). (a) Mean of 12 FluxCom GPP products minus MODIS NPP (see Figure 5), (b) simulated with ISBA_bgc5, (c) simulated with ISBA_bgc6, (d) zonal average observation-derived GPP-NPP and simulated R_a , (e) ISBA_bgc5 minus observation derived, and (f) ISBA_bgc6 minus observation derived.

ISBA_bgc5 (Table 6) especially in the tropical forests and in Eastern North America where the strong overestimation of gross photosynthesis is reduced. For the tropical forests, this is mainly due to the strong reduction in the maximum photosynthetic rate A_{max} (from 2.2 to 0.39 $\text{mgCO}_2/\text{m}^2/\text{s}$; see Table 2) as suggested by the Domingues et al. (2007) values for Amazon species that directly reduce assimilation rates (see equation 3). In general, all forested zones have reduced GPPs with the new version of the model (Figure S1). This is also linked to the reduction in A_{max} deduced from the Kattge et al. (2009) V_{cmax} values using equation 6 resulting in smaller maximum photosynthetic rates for trees (see Table 2). In the boreal forest, GPP is now underestimated. Needleleaf trees in particular, boreal and to a lesser extent temperate, are not productive enough, especially in summer (Figure S2). Here, it is mainly the strong reduction in specific leaf area (SLA see Table 2 from 13.3 to 5.0 m^2/kg) from the TRY database that plays a role. The smaller SLA leads to a smaller area of leaves per unit of carbon assimilated and a reduced area to photosynthesize. To a lesser extent, the reduction in A_{max} (from 2.2 to 1.4 $\text{mgCO}_2/\text{m}^2/\text{s}$) deduced from the Kattge et al. (2009) V_{cmax} values using equation 6 also plays a role. Compared to MODIS-derived GPP, ISBA_bgc6 also overestimates GPP in the tropics and underestimates it in the midlatitude to high latitude (Figure S3).

Autotrophic respiration (R_a) can be roughly calculated as the difference between the observation-derived GPP and NPP. ISBA_bgc5 generally overestimated R_a , especially in the forests (Figure 4b). This bias is greatly reduced by ISBA_bgc6 (Table 6). This improvement is partly due to the improvement in GPP (leaf dark respiration depends on assimilation; see equation 7) but mostly to the modified leaf dark respiration parameterization applied to tree PFTs. Joetzer et al. (2015) showed that ISBA_bgc5 strongly overestimated leaf dark respiration in the Amazon Forest. Following Bonan et al. (2011), they used a vertical profile of leaf

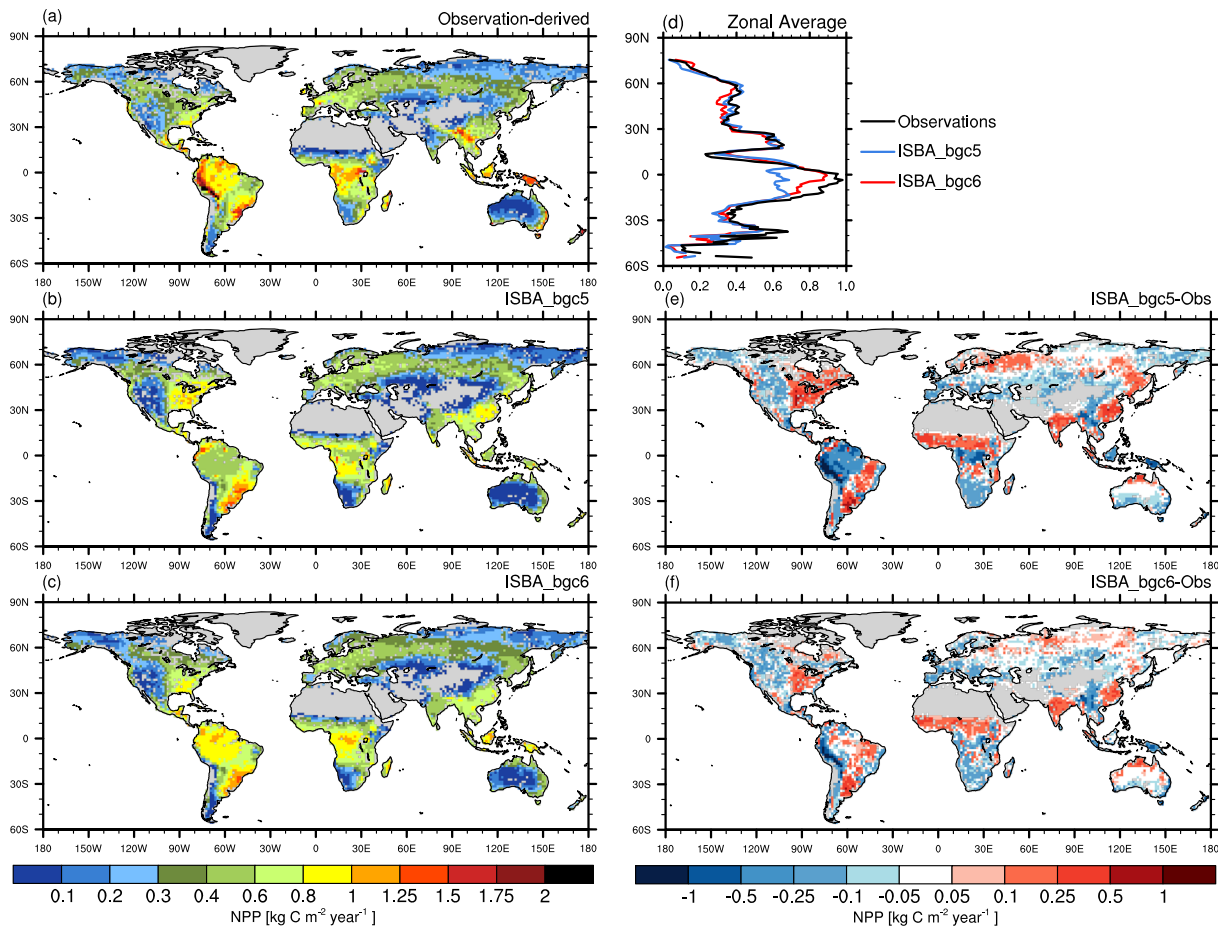


Figure 5. Net primary productivity (NPP). (a) MODIS NPP with the missing data in gray. The same mask is applied to the simulation results: (b) simulated with ISBA_bgc5, (c) simulated with ISBA_bgc6, (d) zonal average observation-derived NPP and simulated, (e) ISBA_bgc5 minus observation derived, and (f) ISBA_bgc6 minus observation derived.

nitrogen applied to dark respiration in the canopy that decreased autotrophic respiration despite the added sapwood respiration that was neglected in ISBA_bgc5. We applied this vertical profile of leaf nitrogen and sapwood respiration to all tree PFTs in ISBA_bgc6 (see section 2.2). As a result, autotrophic respiration decreases in all forests in ISBA_bgc6 compared to ISBA_bgc5 (Figure S4).

NPP is generally improved in all regions of the world compared to MODIS-derived data (Figure 5 and Table 6). This improvement can be traced to the improvement in GPP, mostly a reduction of forest GPP due to the use of updated parameters mentioned above (Figure S5). In tropical forests however, NPP was greatly underestimated by ISBA_bgc5 despite an overestimated GPP. This low NPP was due to the strongly overestimated leaf dark respiration as mentioned above and is corrected by the assumed vertical profile of leaf N (Joetzjer et al., 2015).

The crop NPP map of Monfreda et al. (2008), representative of year 2000 shows that both versions of the model tend to overestimate crop productivity, although slightly less with the new version (Figure 6). In ISBA, crops have physiological parameters distinct from grasses (*Ammx*, *Gmes*, etc.; Table 2), but their phenology depends on the carbon balance of the leaves as it is the case for grasses. There is no planting and harvesting dates which tend to overestimate the crops growing season in most regions of the world and partly explains the overestimation of NPP. One exception to this high crop NPP is Western Europe and is probably due to the fact that ISBA was originally developed and tuned for France and Western Europe (see for instance Canal et al., 2014).

Carbon use efficiency (CUE) is the fraction of assimilated carbon that is used for growth. For plants at the community level, it is calculated as the ratio NPP/GPP (Manzoni et al., 2018). It represents the capacity of

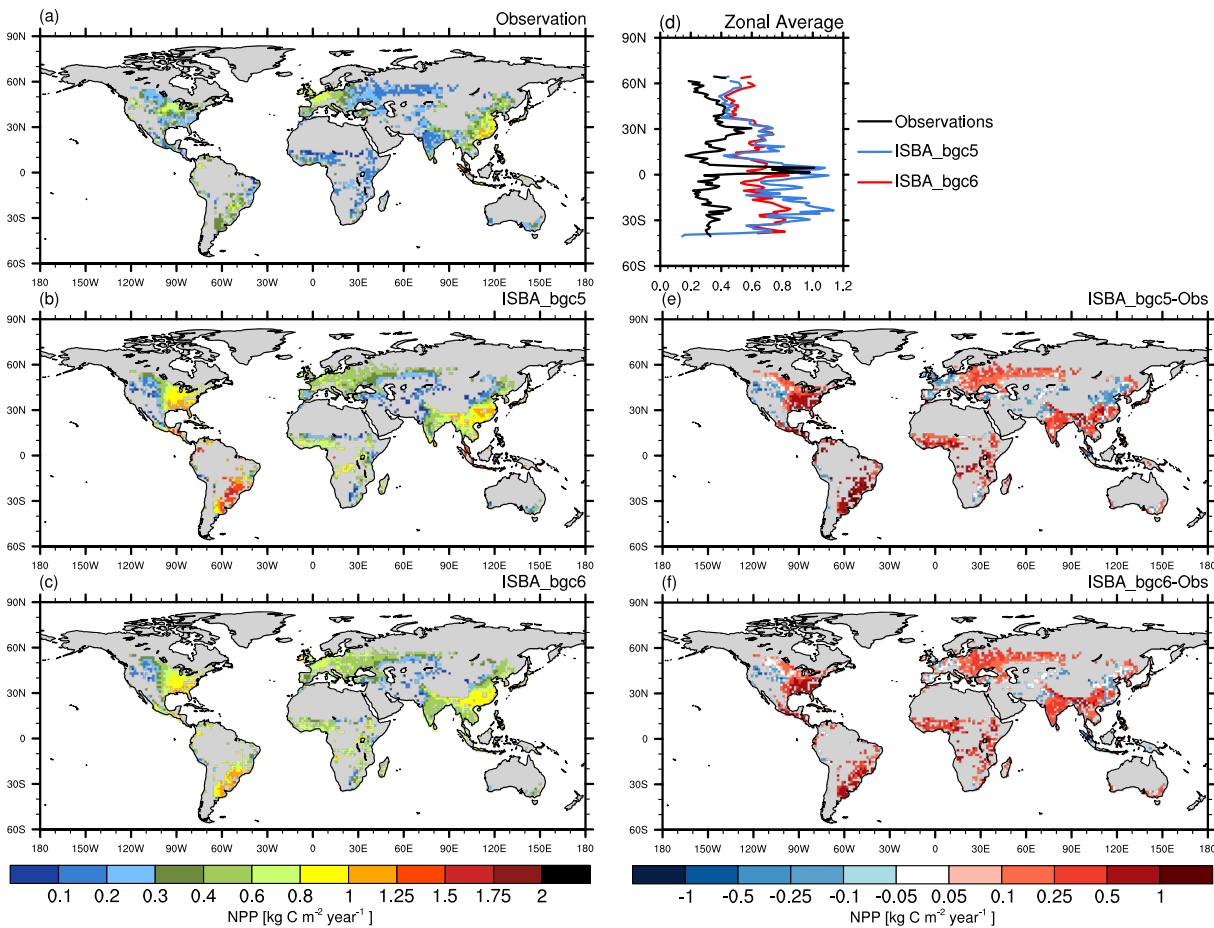


Figure 6. Crop NPP. The value in each grid cell corresponds to the NPP of the crop as if it was covering the whole grid cell. (a) FAO NPP with the missing data in gray. The same mask is applied to the simulation results: (b) simulated with ISBA_bgc5, (c) simulated with ISBA_bgc6, (d) zonal average observation-derived NPP and simulated, (e) ISBA_bgc5 minus observation derived, and (f) ISBA_bgc6 minus observation derived.

an ecosystem to transfer assimilated atmospheric C to biomass and depends on vegetation type, stand age and climate (Delucia et al., 2007; Manzoni et al., 2018; Xia et al., 2017). Being the ratio of the net flux to the input flux to vegetation, it is also a good indicator of the inner working of the model. Despite being a big-leaf model without representation of forest age structure, ISBA_bgc6 simulates tropical evergreen forest with a CUE close to 0.3 that compares reasonably well with data from Malhi et al. (2009) (Figure S6). This is a great improvement from the 0.1 value of ISBA_bgc5 (Joetzjer et al., 2015). In general, the decrease in R_a in forests results in an increase in CUE. Tropical deciduous forest and temperate forests have CUEs from 0.3 to 0.6, within the range reported by Zhang et al. (2014) and He et al. (2018). However, for boreal forests, the decrease in R_a results in CUE values around 0.7, a little higher than the maximum value of 0.65 theoretically derived by Amthor (2000) or much higher than the 0.5 given by Zhang et al. (2014) for high latitudes. ISBA_bgc5 already simulated too high values for boreal ecosystems (Xia et al., 2017), and this bias is reinforced by ISBA_bgc6.

Heterotrophic respiration (R_h): Compared to the estimations of Hashimoto et al. (2015), both versions of the model underestimate heterotrophic respiration (CO_2 emitted by soil C decomposition) in the mid to high latitudes (Figure 7). This has now been traced back to an overestimated lignin content of the litter that reduces the decomposition rate in the CENTURY model. ISBA_bgc6 overestimates heterotrophic respiration in the Tropics compared to Hashimoto's work. This is the result of the changes in carbon cycling in tropical forests as described in Joetzjer et al. (2015): the reduced autotrophic respiration increases NPP, leading to increased litterfall and larger litter and soil carbon pools (see section 4.3, Figure S7). The resulting heterotrophic respiration around $0.8 \text{ kgC/m}^2/\text{year}$ is coherent with in situ observations from the Amazon

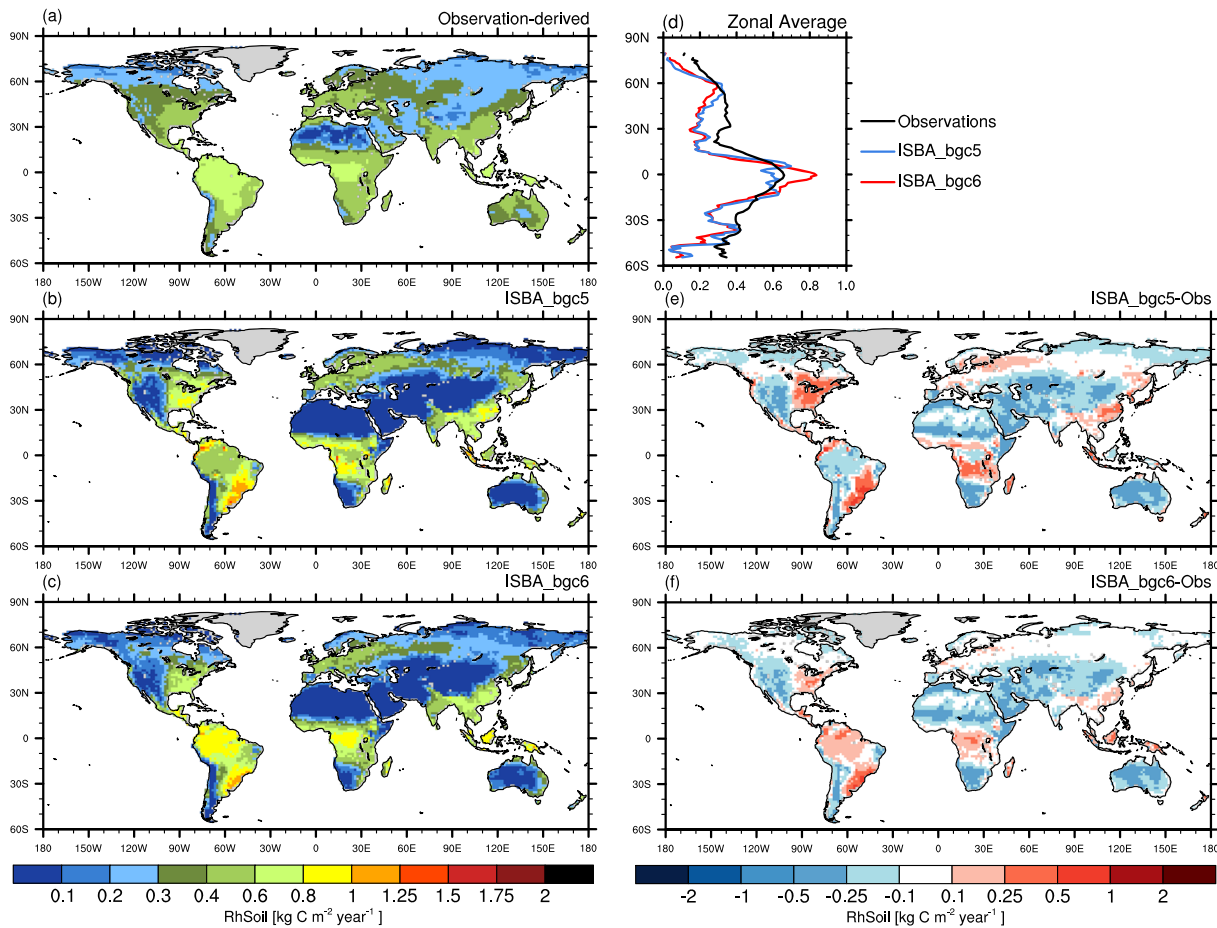


Figure 7. Heterotrophic respiration (Rh). (a) Hashimoto et al. (2015) data, (b) simulated with ISBA_bgc5, (c) simulated with ISBA_bgc6, (d) zonal average observation derived and simulated, (e) ISBA_bgc5 minus observation derived, and (f) ISBA_bgc6 minus observation derived.

(0.8–1.5 kgC/m²/year, Malhi et al., 2009) but higher than the values around 0.6 deduced by Hashimoto et al. (2015).

Fire and carbon-induced fire emissions were not represented in ISBA_bgc5. The emissions are calculated in ISBA_bgc6 based on the computed burned area (section 2.8). The model reproduces correctly the overall distribution of fires with the largest percentage of burned land in semiarid regions, mostly the Sahel and S-E Brazil, peaking around 10°N and 15°S (Figure 8). The model overestimates burned areas in the Southern Hemisphere and the North American South West. Globally and averaged over 1981–2000, ISBA_bgc6 simulates 4.37% compared to the 4.26% estimated by Mouillot and Field (2005). Fire-induced carbon emissions follow this area distribution with peaks of emissions around 10°N and 15°S (Figure 9), but emissions are largely overestimated especially in the S Hemisphere compared to van der Werf et al. (2017). Globally, these fluxes of C are small compared to NPP (2 or 3 PgC/year compared to 45 PgC/year). But in fire prone areas like the Sahel, carbon emissions due to fire may account for up to one fourth of local NPP, and the fire module should be revised in the future.

DOC originating from soil carbon leaching and its transport by the river system is only simulated in ISBA_bgc6. We compare the simulated leached C with the yield map of DOC from the NEWS2 observation-derived product (Mayorga et al., 2010). The DOC yield corresponds to the total mass flux of DOC exported by the river divided by the river basin area (Figure 10a). The largest DOC sources are the Amazon Basin and Indonesia, S-E Asia, tropical Africa, and the midlatitude to high latitude of the Northern Hemisphere. Qualitatively speaking, the model presents similar patterns with the highest C leaching fluxes in the Amazon Basin, Indonesia, S-E Asia, and to a lesser extent, the boreal forest (Figure 10b). The largest fluxes of DOC are simulated in regions where heterotrophic respiration is high.

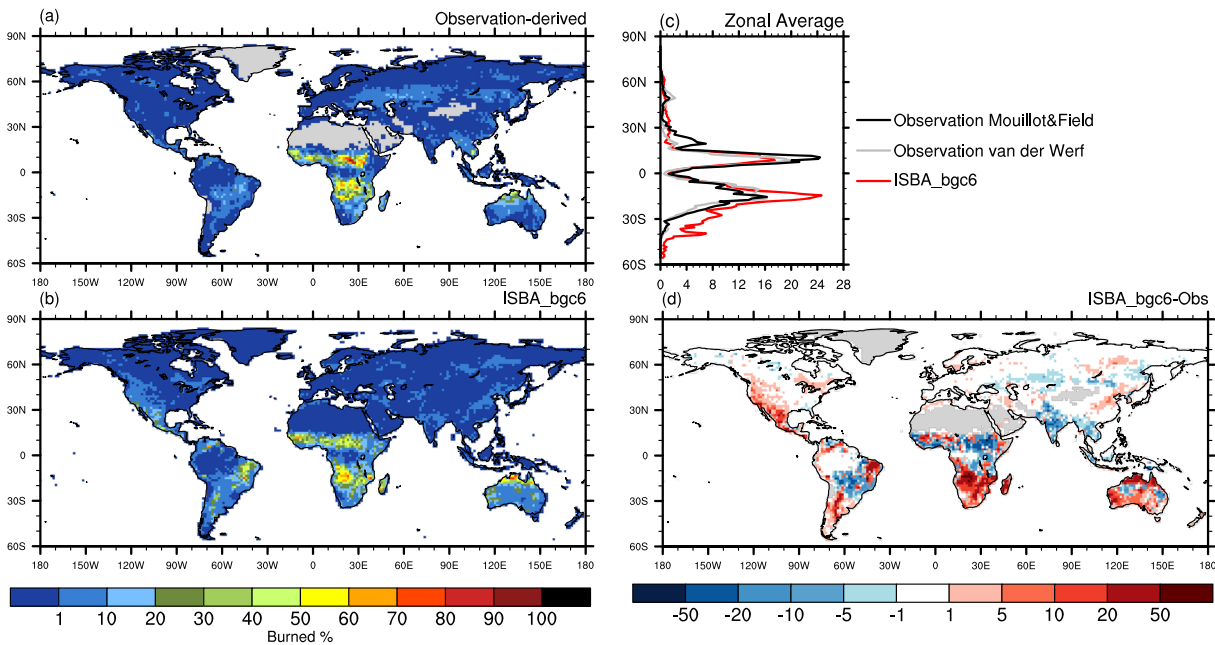


Figure 8. Fraction of grid cell burned each year (in %). (a) Mouillot and Field (2005) product with missing data in gray. The same mask is applied to the simulation results: (b) simulated with ISBA_bgc6, (c) @zonal averages of simulation and of the Mouillot and Field and the Van der Werf GEFD4 data, and (e) ISBA_bgc6 minus observation-derived (Mouillot & Fied, 2005).

This was expected since we assumed that the mobilization of DOC is controlled by the same environmental factors as decomposition in the model (see section 2.9). In the Amazon, C leaching from the soil is high because temperature and soil moisture conditions are favorable for decomposition. In the high latitudes, C leaching is high despite low decomposition rates because soil C content is high. Compared to the Mayorga et al.'s data set, the amounts however are smaller (Table 6 and Figure 10). This was expected because we deliberately chose to get the right order of magnitude delivered to the open ocean without simulating the removal processes in rivers and estuaries.

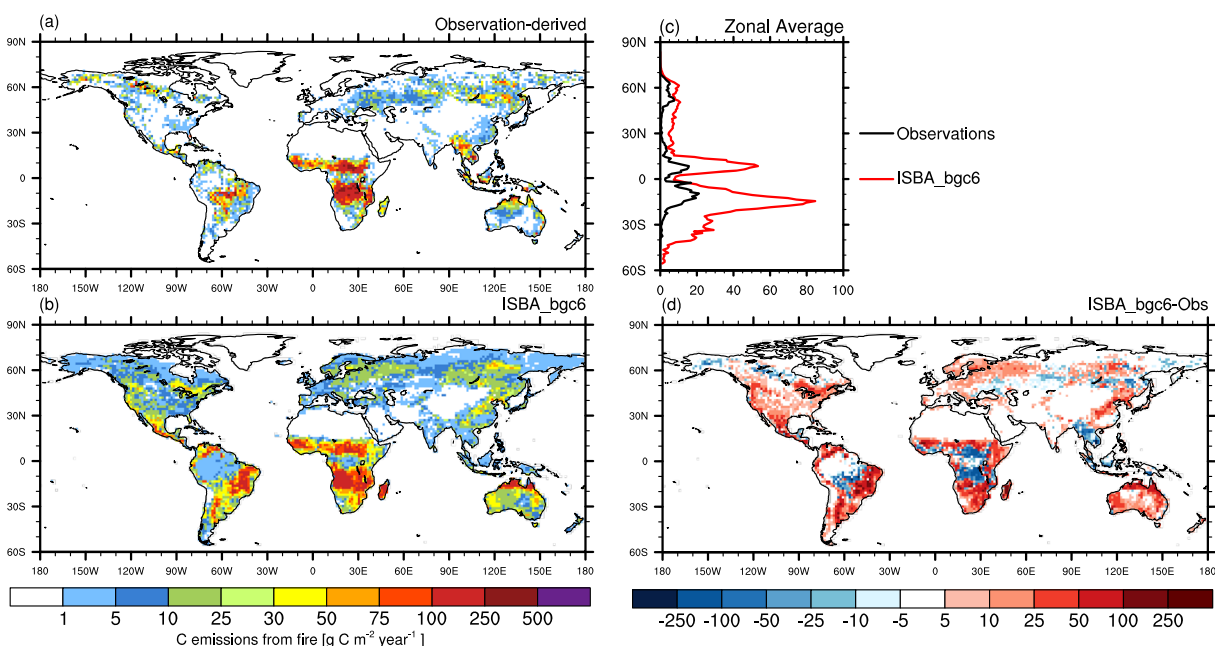


Figure 9. Carbon emissions from fire. (a) GEFD4 product, (b) simulated with ISBA_bgc6, (c) zonal averages, and (d) ISBA_bgc6 minus observation derived.

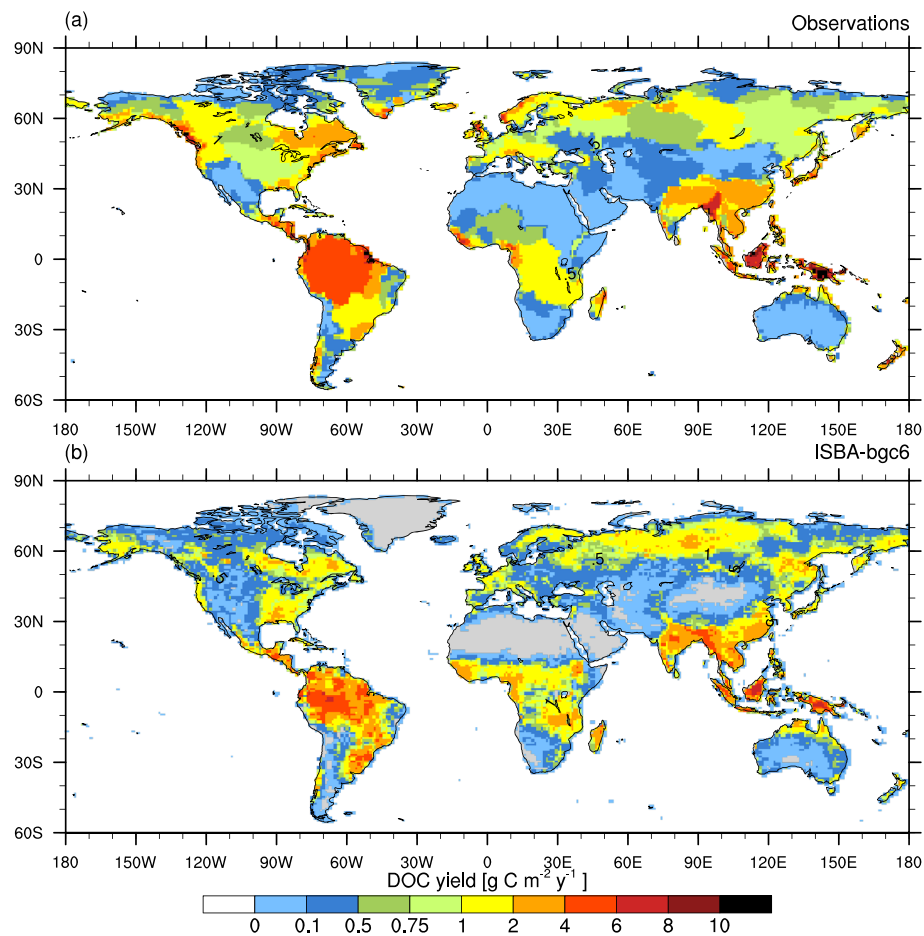


Figure 10. Dissolved organic carbon yield (leached from the soil). (a) Mayorga et al. (2010) product given per major river basin and (b) simulated with ISBA_bgc6

Compared with the available data for the largest rivers of the world, ISBA-CTRIP simulates well the total yearly DOC flux over the whole river basin (Figure 11). However, as mentioned by Dai et al. (2012), it is obvious that this flux is mostly dependent on river discharge, well simulated by ISBA-CTRIP (see

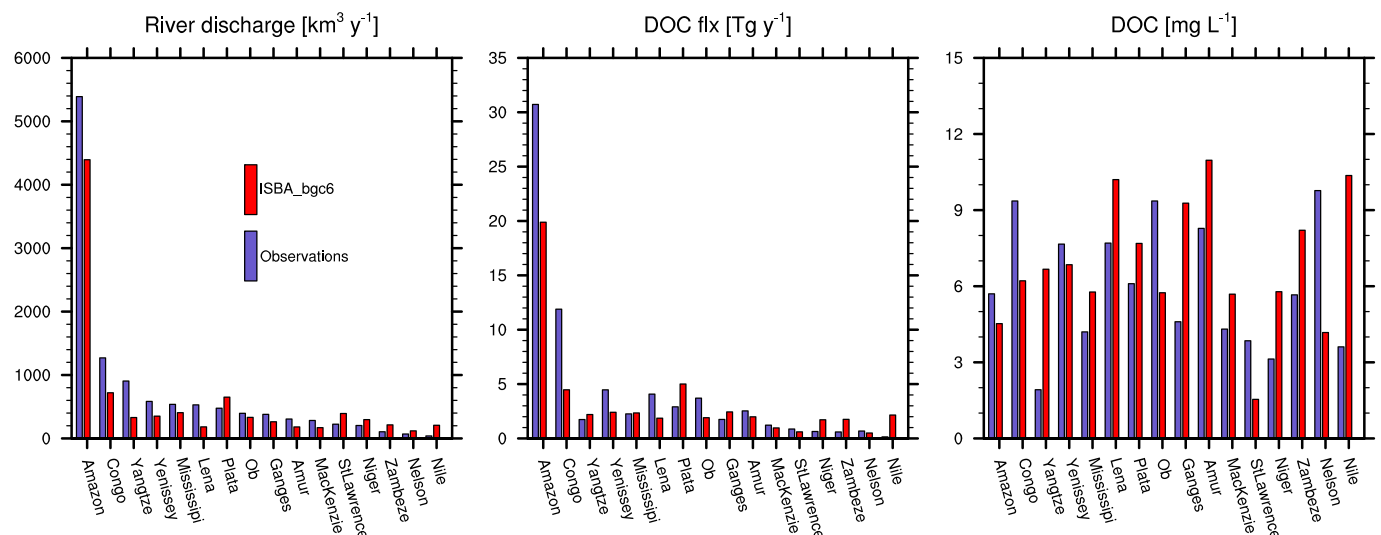


Figure 11. (a) River discharges, (b) DOC flux, and (c) DOC concentration of some the largest rivers in the world.

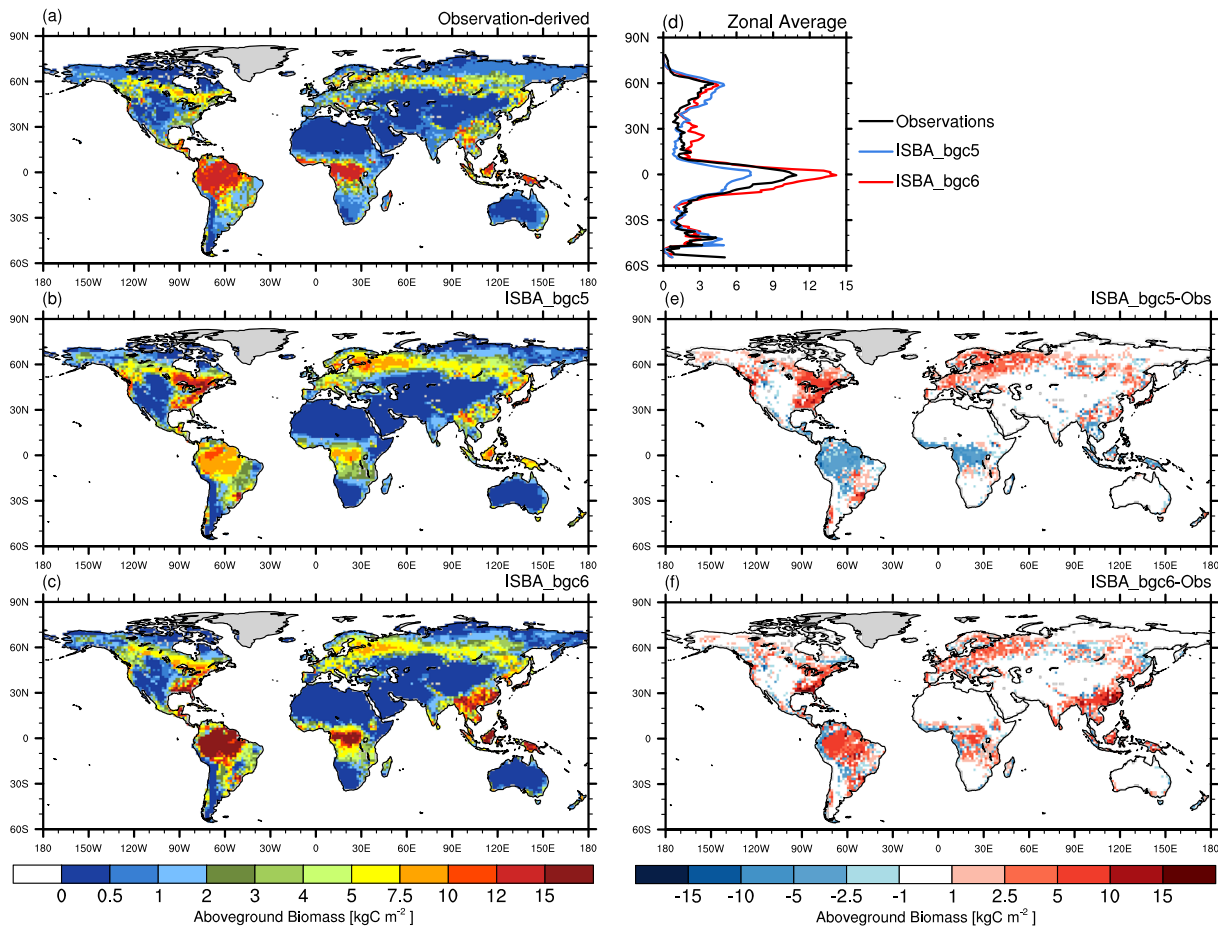


Figure 12. Aboveground biomass. (a) Liu et al. (2015) data set, (b) simulated with ISBA_bgc5, (c) simulated with ISBA_bgc6, (d) zonal averages, (e) ISBA_bgc5 minus observation derived, and (f) ISBA_bgc6 minus observation derived.

Decharme et al., 2019 for a detailed analysis of ISBA-CTrip hydrology). For most large rivers the simulated DOC flux is smaller than the observed. Again, this is expected since we wanted the right amount reaching the open ocean without representing the removal processes in the estuaries that may remove from 2% to 30% from the rivers (see Dai et al., 2010 and references within).

DOC concentration on the other hand is more indicative of the processes, and as expected, our very simple parameterization is not sufficient to correctly represent the observed variability in DOC concentration between rivers. Some of the largest DOC concentrations are seen in the Arctic rivers (Yenisey, Lena, and Ob) that drain permafrost C rich area. As mentioned earlier, ISBA simulates the highest soil C stores in the high latitudes but fails to represent some of the very high carbon contents from Scandinavia to Eastern Siberia, including the large swamps and peat bogs in the Ob River Basin or in Canada. The model simulates correctly permafrosted soils from the physical point of view (see Decharme et al., 2019) with a coherent vertically discretized solution of both Fourier and Darcy's laws. Soil biogeochemistry however is not discretized and uses the average temperature and soil water content over the first meter of soil to calculate decomposition rates and soil C mobilization. This affects the amount of C decomposed and leached and can be seen mostly during the thawing and freezing phases (see Morel et al., 2019). Moreover, the model currently represents upland C processes, while the largest stores are located in wetlands.

4.2. Carbon Pools

4.2.1. Vegetation biomass

Aboveground biomass in ISBA is calculated as the sum of leaves, stem/twigs, trunk, and the numerical storage pool. Overall, the distribution of aboveground biomass reflects the forest distribution (Figure 12). Compared to the Liu et al. (2015), both versions of the model tend to overestimate biomass in the boreal

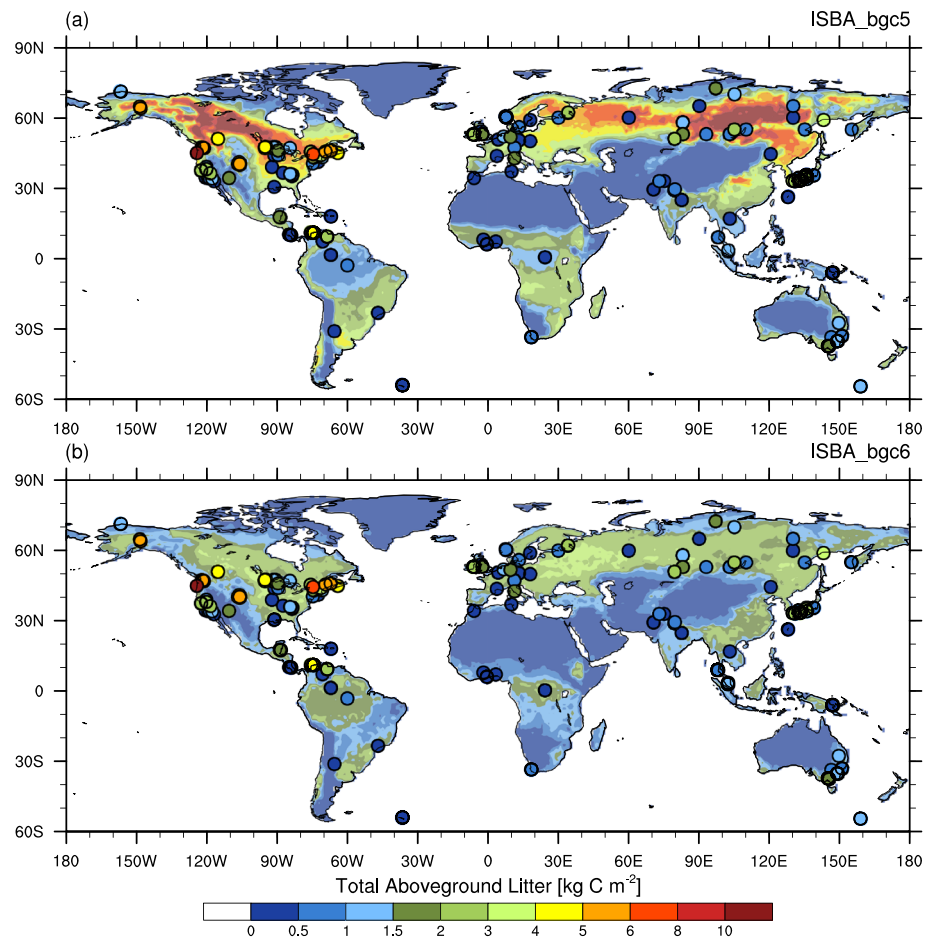


Figure 13. Aboveground litter pool. In situ observations from Holland et al. (2015) excluding reported management in circles and simulated results in background. (a) Simulated with ISBA_bgc5 and (b) simulated with ISBA_bgc6.

and temperate forests, although slightly less with ISBA_bgc6 (Figure S8). Data using radar data give even lower estimates for temperate and boreal forest aboveground biomass (Table S1) indicating room for improvement in the model (Thurner et al., 2014). Following the changes in NPP, tropical evergreen forests where biomass was too low with bgc5 (Figure 12e) have now too much aboveground carbon (Figure 12f and Table S1; Baccini et al., 2012; Saatchi et al., 2011). This general overestimation of aboveground biomass is partly due to an insufficient allocation to roots in forested ecosystems by ISBA_bgc6 (and ISBA_bgc5). Instead of a ratio of total biomass to aboveground biomass (TBC/ABC) around 1.26 for tropical forests and 1.24 for temperate and boreal forests as suggested by Liu et al., 2015 based on literature review, ISBA_bgc6 results in TBC/ABC ratios of 1.21, 1.13, and 1.11. Another reason for the overestimation of woody biomass is the very simple representation of mortality as a constant turnover for the stem and coarse root pools. The only disturbances considered are fire and land cover change in the case of ISBA_bgc6.

4.2.2. Litter Pools

There are very few data sets on aboveground litter, let alone belowground litter, to evaluate models. One exception is the “Global Database of Litterfall Mass and Litter Pool Carbon and Nutrients” (Holland et al., 2015) including site measurements of among others aboveground litter carbon dating from 1827 to 1997. To compare our simulation results, we excluded data with reported management. Overall, ISBA_bgc6 simulates much less aboveground litter (Figure 13) than ISBA_bgc5 (Figure S9) and has values that are more in the range of the in situ observations on all continents, except N America. This reduction in aboveground litter is mainly due to the effect of fire that consumes aboveground litter (see section 2.8) and was not represented in ISBA_bgc5. The tropical forest is the only biome with increased aboveground

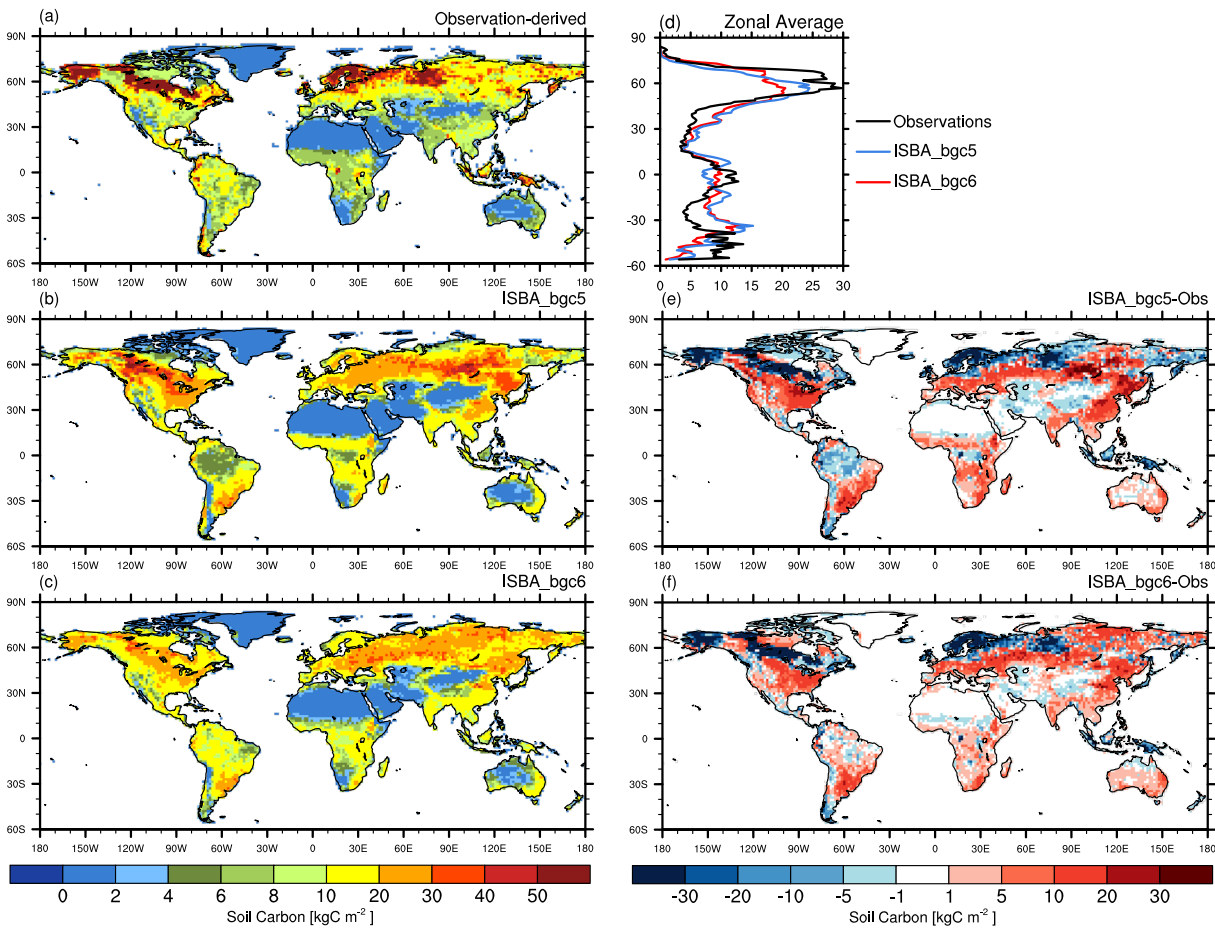


Figure 14. Soil carbon content. (a) HWSDv1.2, (b) simulated with ISBA_bgc5, (c) simulated with ISBA_bgc6, (d) zonal averages, (e) ISBA_bgc5 minus observation-derived, and (f) ISBA_bgc6 minus observation-derived.

litter because NPP and hence litterfall have increased while humidity limits fire. Belowground litter is very similar between the two versions of the model (Table 5).

4.2.3. Soil organic carbon

Compared to the observations to 1-m depth, both versions of the model strongly underestimate soil organic matter in the Ob basin, Scandinavia, along the Laurentian lakes and in Alaska (Figure 14). These pools however are in permafrost area and result from the history of climate since the last deglaciation. As such, they cannot and should not be reproduced with a land surface model forced by present day climate. However, even with a realistic climate forcing for the whole deglaciation and Holocene, ISBA_bgc6 would not be able to correctly represent soil organic matter in the high latitudes because it is missing some important processes (Guimberteau et al., 2018). CENTURY's bulk approach of soil carbon does not allow a detailed vertical representation of the carbon that is frozen and thawed, as mentioned in the section on DOC. The model also does not represent bioturbation and cryoturbation, the processes responsible for carbon mixing in the soil (Koven et al., 2013). It also does not represent peat soils. In the tropical forests, the negative bias in soil carbon of ISBA_bgc5 is mostly corrected with ISBA_bgc6 due to the higher NPP resulting in higher turnover, the input flux to the litter and soil carbon pools. In the other regions, both versions of the model tend to overestimate soil carbon under forest and croplands, although slightly less with ISBA_bgc6 thanks to the reduction in non-tropical forest NPP (Figure S10). This is in part related to the overestimated lignin content as mentioned earlier. In managed lands, the too large soil carbon is partly explained by the fact that neither version of ISBA represent grazing in pastures and crop harvesting. The amount of litterfall in managed land is therefore overestimated resulting in a too large input flux to the soil carbon pool.

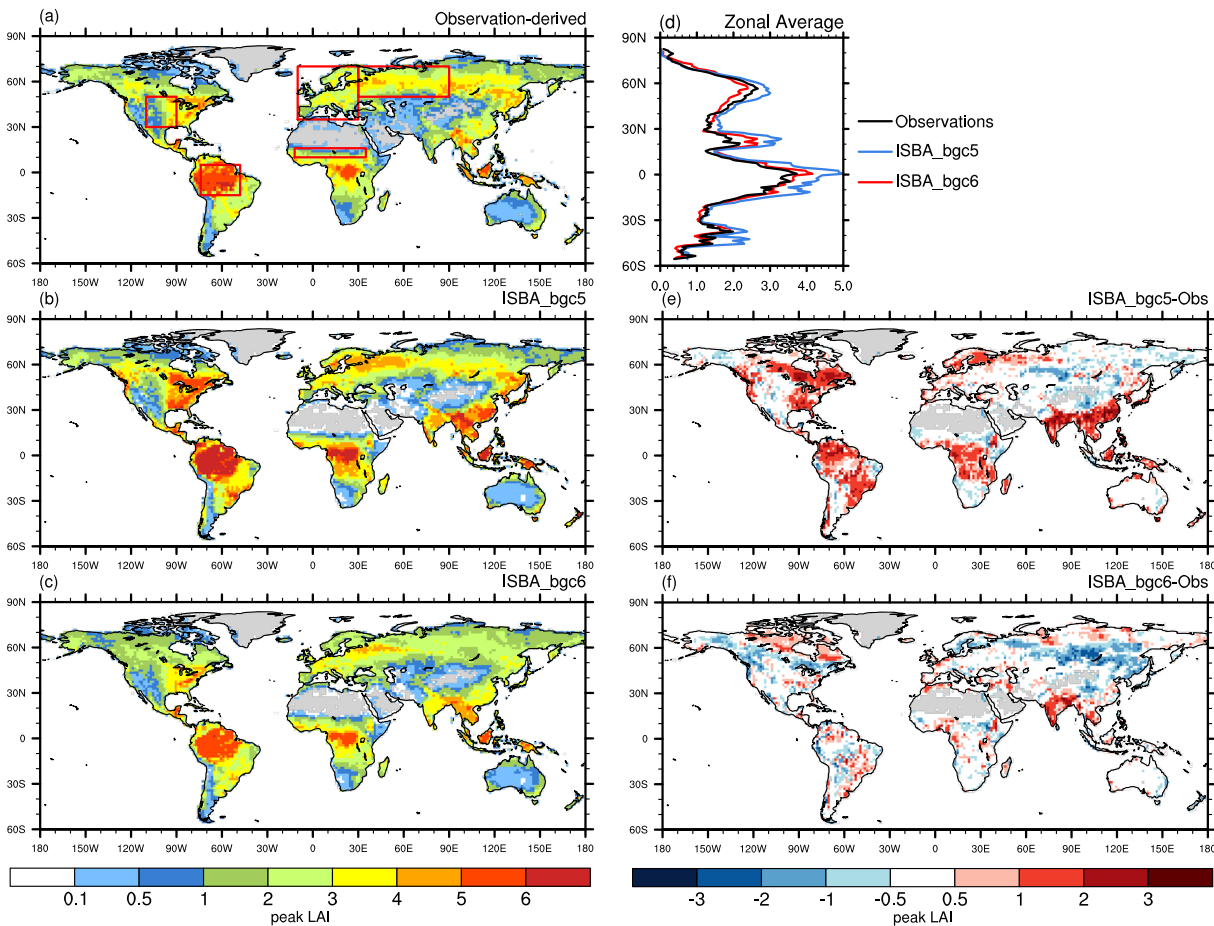


Figure 15. Peak LAI calculated from the average seasonal cycle. (a) LAI3g product, (b) simulated with ISBA_bgc5, (c) simulated with ISBA_bgc6, (d) zonal averages, (e) ISBA_bgc5 minus observation derived, and (f) ISBA_bgc6 minus observation derived. The red lines in (a) delineate the regional masks used in Figure 16.

ISBA_bgc6 simulates overall less soil organic carbon than ISBA_bgc5 (Table 5). The decrease comes mainly from the boreal, temperate forests, and, to a lesser extent, dry tropical forests and is related to the reduction in aboveground litter. Tropical forest soil carbon has increased again because of the increased NPP in the region. Tundra has also increased soil carbon content with ISBA_bgc6, due to the slightly increased NPP and the lack of fire.

4.3. Vegetation and Soil Turnover Time

Turnover times, estimated as the ratio of a carbon pool to its input flux, may be used as tool to understand how a model might behave in climate change simulations in terms of carbon cycling (Koven et al., 2015; Wu et al., 2018). Here, we chose to estimate vegetation turnover time as biomass/NPP and soil turnover time as “dead carbon”/NPP, where dead carbon represents litter and soil carbon. To be exact, turnover times should be evaluated at equilibrium. But to be able to compare them with the available data set, we use the last 30 years of our simulations. The input flux to the litter and soil carbon pool should be the mortality flux (dead leaves, branches, plants), not available from data. However, at equilibrium, this flux is equal to NPP. This is why we estimate soil turnover time as the ratio of litter and soil carbon to NPP. Much care should be however taken with the observation derived turnover times since they are calculated as ratios of not necessarily coherent satellite-based estimates.

For vegetation, the model tends to overestimate turnover time in cropland and forests with the exception of tropical Africa (Figure S11) and underestimate it in grasslands, especially in drylands (central Australia, Sahel, Brazil’s Nordeste). This overestimation is coherent with the fact that the model does not represent

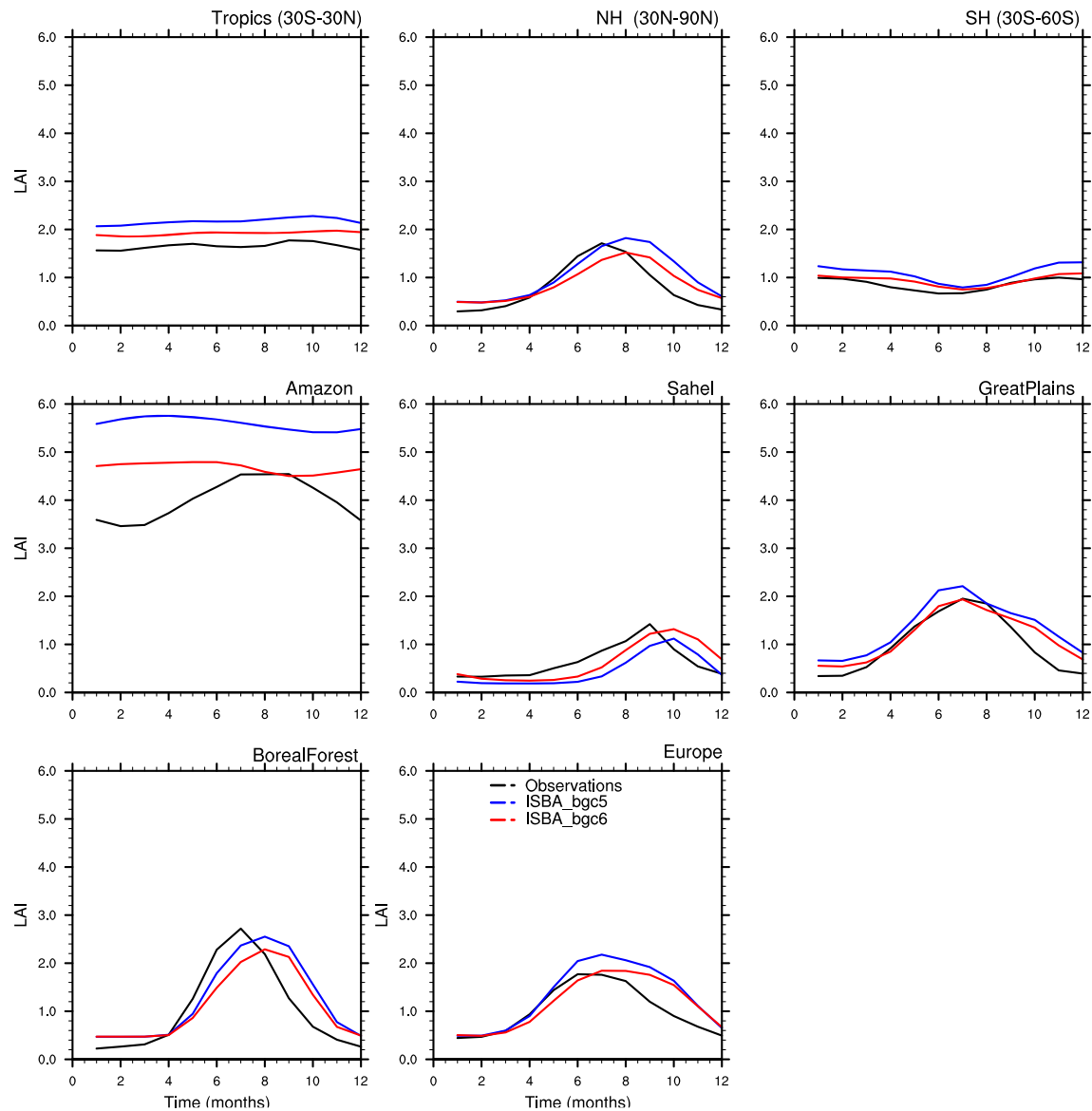


Figure 16. Regional average seasonal cycle of LAI from the LAI3g product and simulated by ISBA_bgc5 and ISBA_bgc6. See Figure 15a for the regional masks.

disturbance mortality explicitly for forests and harvest for croplands. For grasslands, it is more complex to interpret in part because the biomass reservoir is smaller and the ratio is more sensitive to uncertainties in the fluxes and pools. For soils, the turnover bias map is rather similar to the soil carbon bias map: positive biases almost everywhere except in the peat soils in the high latitudes.

The improvements in NPP, biomass, and soil carbon between the two versions of the model translate into turnover times. However, some features of the biases are mainly explained by missing processes such as forest disturbances and crop harvest for vegetation turnover times (Figure S11) and peat carbon for soil turnover times (Figure S12).

4.4. Leaf Phenology

4.4.1. Peak LAI

LAI has a strong effect on surface energy, water, and especially carbon fluxes because it determines the area of leaves that absorbs and reflects radiation, may photosynthesize and transpire. Contrary to most land surface models, there is no phenology model in ISBA, and LAI is directly the result of the leaf carbon balance. As such, LAI is both a major determinant and a result of carbon fluxes. Peak LAI, calculated as the maximum of

Table 7
Global Fluxes Averaged Over Years 2006–2015 and Linear Trends Over Years 1960–2015

	ISBA_bgc5		ISBA_bgc6	
	2006–2015, mean	1960–2015, linear trend	2006–2015, mean	1960–2015, linear trend
GPP	140.7	0.535	117.1	0.299
NPP	49.1	0.141	49.8	0.113
Ra	91.69	0.394	67.25	0.187
Rh	45.06	0.101	43.62	0.089
DOC flux	-	-	0.077	$-5.5 \cdot 10^{-5}$
Fire C	-	-	2.711	$-8.7 \cdot 10^{-4}$
fLCC	-	-	1.11	$3.4 \cdot 10^{-3}$
NEP ^a	4.03	0.039	6.20	0.023
NBP ^b	4.03	0.039	2.31	0.02

Note. Total fluxes are in PgC/year and linear trends in PgC/year².
^aNEP = NPP-Rh ^bNBP = NEP-DOC-FireC-fLCC.

the average seasonal cycle of monthly LAI, is reduced in ISBA_bgc6 compared to ISBA_bgc5, mostly over forests, especially tropical but also boreal (Figures 15d and S13). Compared to the LAI3g, this reduced peak LAI is an improvement in the tropics, India and S-E Asia where the model used to overestimate LAI (Figures 15e and 15f). In the boreal forest, ISBA_bgc6 now slightly underestimates peak LAI, from the Pacific NW to central and E Siberia. For most vegetation types, the smaller peak LAI is related to the reduced maximum photosynthetic rate *Ammax*, decreasing GPP and NPP and hence LAI, as it results from the carbon balance of the leaves. In the tropical forests, where NPP is actually increasing, the reduced peak LAI is mostly due to the drop in SLA (14.6–8.3 m²/kg) suggested by the TRY database for tropical evergreen trees. In the boreal forests the strong reduction in specific leaf area for conifers, both boreal and temperate (from 13.3 to 5.0 m²/kg) from the TRY database also plays a major role that adds up to the reduction in *Ammax*.

4.4.2. Amplitude and phase

Figure 16 shows the average seasonal cycle for large regions, Northern Hemisphere and Southern Hemisphere extratropics, the tropics, and some specific regions: the Amazon, the Sahel, the Great Plains, and the Eurasian Boreal forest. With the exception of the Amazon Basin, the amplitude and phase of the cycle are well reproduced by the model, especially with ISBA_bgc6. However, the month of the peak and the timing of senescence are delayed by 1 month, whatever the model version or atmospheric forcing. This might be related to the calculated leaf longevity in ISBA. The amplitude of the seasonal cycle in the Amazon Basin is too small compared to the LAI3g product and out of phase. This is because leaf phenology in the Amazon does not depend only on the carbon balance of the leaves (see Joetzjer et al., 2015 for a discussion).

4.5. Flux Trends

We assess the trends of the simulated carbon fluxes because of their relevance for the carbon budgets (Le Quéré et al., 2018). Whatever the model version, the largest positive trends are simulated for GPP (Table 7), representing the “input” flux to the system. This increase in carbon assimilation is due to the CO₂ fertilization effect, the increase in water use efficiency for water-limited ecosystems and to more favorable climate conditions like a longer growing season at high latitudes. The fertilization effect and the increased water use efficiency are directly the result of the increased atmospheric CO₂ concentration. ISBA_bgc5 had a very high fertilization effect that was strongly reduced in ISBA_bgc6 because of the dependency of SLA on CO₂ concentration and the ad hoc downregulation parameterization (see section 2.5). As mentioned earlier, changes in the other main fluxes (NPP, Rh, etc.) respond mostly to the changes in GPP and the trends are more modest. These trends however are hard to evaluate. The trend of our simulated land net carbon uptake (NBP) compares favorably with the estimated value of 0.03 +/- 0.02 PgC/year² reported by Ciais et al. (2019) for the trend in the total land carbon sink from 1960 to 2016. As it is the case with most land surface models, ISBA simulates a positive trend in the net carbon flux because the increase in photosynthesis (GPP) is larger than the increase in autotrophic and heterotrophic respiration. However, contrary to what is reported by Bond-Lamberty et al. (2018), ISBA does not simulate an increasing trend of the ratio of Rh to GPP and might therefore overestimate the terrestrial sink in the future.

5. Summary and Conclusions

The carbon cycling module of ISBA was greatly/largely updated throughout the 2010 decade. The model now takes into account land cover changes, wild fires, and leaching of carbon from the soil, processes that were neglected in previous versions. The existing processes were also revised, mainly modifying tree leaf dark respiration and using the TRY database for updating photosynthesis and leaf traits parameters. The comparison of the results of two versions of the model with a present-day atmospheric forcing shows that the gross vegetation carbon fluxes (GPP and Ra) are greatly improved through mainly a general decrease in GPP and a strong decrease in Ra for trees. The net flux NPP is also improved mainly for tropical forests. Vegetation

biomass has increased in the tropics where it was underestimated, and the high bias is reduced in the midlatitude to high latitude. The amplitude of the average seasonal cycle of LAI is also improved with ISBA_bgc6, mostly due to a reduced peak LAI. The phase of the seasonal cycle is well reproduced by the two versions of the model despite a 1-month delay for the timing of peak LAI and senescence. For the litter and soil compartments, the most striking change is seen in the aboveground litter pool that is almost reduced in half, especially in the mid to high latitudes. Fires are the main reason for this strong reduction. Soil carbon is improved in the tropical rainforests but is generally overestimated in midlatitudes, slightly less with ISBA_bgc6. The trends of the carbon fluxes are also reduced with ISBA_bgc6, and the trend of the net flux (NBP) is comparable to published estimates.

The newly represented processes have little impact on the global carbon fluxes. Fire carbon emissions, LCC related emissions, and DOC flux together are one to two orders of magnitude smaller than photosynthesis and respiration. They are also smaller than the change in global GPP due to the updated parameters (117 vs. 140 pgC/year). They are however of the same order of magnitude as the net ecosystem production and are crucial to get a reasonable estimate of the land carbon sink. They also affect other fluxes and pools, like the reduction of aboveground litter due to fire. But they are also needed when running in coupled mode within the Earth System Model CNRM-ESM as DOC is one of the main inputs of C to the global ocean (Resplandy et al., 2018) and fires and LCC also affect the physical climate (see for instance Saha, D'Odorico, & Scanlon, 2017 for fire and De Noblet-Ducoudré et al., 2012 or Lawrence & Chase, 2010 for LCC).

The results of this comparison indicate several areas of improvement for the ISBA biogeochemical module. The satellite-derived and ecological data suggest that the model underestimates the productivity of boreal forests and overestimates their CUE, pointing to possible improvements in the representation conifers. The overestimation of crop NPP compared to the census-based data indicates the need to take into account a distinct crop phenology. The overall overestimated tree biomass shows the need to better represent disturbances and in particular mortality only represented by turnover. In order to correctly represent the carbon cycling in the high latitudes and the CH₄ emissions, the vertically discretized biogeochemical soil carbon module developed by Morel et al. (2019), currently used on arctic peat sites, should be extended and tested on upland sites and applied to the whole boreal and arctic regions. Work should also be done on the seasonal cycle of LAI to improve the timing of the peak and senescence. The very simple fire module, representation of nutrient limitation, and DOC yield modules should also be improved. Despite these caveats, the comparison of the simulated present-day mean carbon fluxes and pools with the available observation-derived data from the arctic to the tropics gives us confidence that the model correctly represents the main processes involved in the terrestrial carbon cycle. The trends of the global fluxes over the last 50 years, at least for the net land biosphere sink, are in agreement with other global models and with the available estimates suggesting that the combined response of the processes to the CO₂ increase and changing climate is reasonable.

References

- Ainsworth, E. A., & Long, S. P. (2005). What have we learned from 15 years of free-air CO enrichment (FACE)? A meta-analytic review of the responses of photosynthesis, canopy properties and plant production to rising CO₂. *The New Phytologist*, *165*, 351–372.
- Akagi, S. K., Yokelson, R. J., Wiedinmyer, C., Alvarado, M. J., Reid, J. S., Karl, T., et al. (2011). Emission factors for open and domestic biomass burning for use in atmospheric models. *Atmospheric Chemistry and Physics*, *11*, 4039–4072. <https://doi.org/10.5194/acp-11-4039-2011>
- Alkama, R., & Cescatti, A. (2016). Biophysical climate impacts of recent changes in global forest cover. *Science*, *351*(6273), 600–604. <https://doi.org/10.1126/SCIENCE.AAC8083>
- Amthor, J. S. (2000). The McCree–de Wit–Penning de Vries–Thornley respiration paradigms: 30 years later. *Annals of Botany*, *86*, 1–20. <https://doi.org/10.1006/anbo.2000.1175>
- Arora, V. K., Boer, G. J., Christian, J. R., Curry, C. L., Denman, K. L., Zahariev, K., et al. (2009). The effect of terrestrial photosynthesis down regulation on the twentieth-century carbon budget simulated with the CCCma Earth System Model. *Journal of Climate*, *22*, 6066–6088. <https://doi.org/10.1175/2009JCLI3037.1>
- Baccini, A., Goetz, S. J., Walker, W. S., Laporte, N. T., Sun, M., Sulla-Menashe, D., et al. (2012). Estimated carbon dioxide emissions from tropical deforestation improved by carbon-density maps. *Nature Climate Change*, *2*, 182–185. <https://doi.org/10.1038/nclimate1354>
- Bastos, A., Friedlingstein, P., Sitch, S., Chen, C., Mialon, A., Wigneron, J.-P., et al. (2018). Impact of the 2015/2016 El Niño on the terrestrial carbon cycle constrained by bottom-up and top-down approaches. *Philosophical Transactions of the Royal Society B: Biological Sciences*, *373*(1760), 20170304. <https://doi.org/10.1098/rstb.2017.0304>
- Bonan, G. B. (2008). Forests and climate change: Forcings, feedbacks, and the climate benefits of forests. *Science*, *320*, 1444–1449. <https://doi.org/10.1126/science.1155121>

Acknowledgments

The authors would like to thank Stephanie Faroux, and Marie Minvielle from the CNRM for their important scientific and technical work on the SURFEX modeling platform. The authors are also grateful to the anonymous reviewers. This research was supported by the “Centre National de Recherches Météorologiques” (CNRM) of Météo-France and the “Centre National de la Recherche Scientifique” (CNRS) of the French research ministry, the H2020 project CRESCENDO Coordinated Research in Earth Systems and Climate: Experiments, Knowledge, Dissemination and Outreach, which received funding from the European Union Horizon 2020 research and innovation program under grant agreement no 641816. It was also supported by the Acceleration of Permafrost Thaw (APT) project through BNP Paribas Foundation, grant number 2014-00000004300 and the “Global Earth Observation for integrated water resource assessment” (earth2Observe) project funding from the European Union Seventh Framework Programme (FP7/2007-2013) under grant agreement No. 603608. The ISBA code used for this work is embedded in the SURFEX numerical interface (Masson et al., 2013) available freely at <https://www.umr-cnrm.fr/surfex/>. The forcing data used for the simulations are available at <http://rda.ucar.edu/datasets/ds314.3/>. The evaluation data sets are available online at addresses given directly in section 33.

- Bonan, G. B., Lawrence, P. J., Oleson, K. W., Levis, S., Jung, M., Reichstein, M., et al. (2011). Improving canopy processes in the community land model version 4 (CLM4) using global flux fields empirically inferred from FLUXNET data. *Journal of Geophysical Research*, *116*, G02014. <https://doi.org/10.1029/2010JG001593>
- Bonan, G. B., Oleson, K. W., Fisher, R. A., Lasslop, G., & Reichstein, M. (2012). Reconciling leaf physiological traits and canopy flux data: Use of the TRY and FLUXNET databases in the community land model version 4. *Journal of Geophysical Research*, *117*, G02026. <https://doi.org/10.1029/2011JG001913>
- Bond-Lamberty, B., Bailey, V. L., Chen, M., Gough, C. M., & Vargas, R. (2018). Globally rising soil heterotrophic respiration over recent decades. *Nature*, *560*(7716), 80–83. <https://doi.org/10.1038/s41586-018-0358-x>
- Calvet, J.-C. (2000). Investigating soil and atmospheric plant water stress using physiological and micrometeorological data. *Agricultural and Forest Meteorology*, *103*, 229–247.
- Calvet, J. C., Noilhan, J., Roujean, J. L., Bessemoulin, P., Cabelguenne, M., Olioso, A., & Wigneron, J. P. (1998). An interactive vegetation SVAT model tested against data from six contrasting sites. *Agricultural and Forest Meteorology*, *92*, 73–95.
- Calvet, J.-C., Rivalland, V., Picon-Cochard, C., & Guehl, J.-M. (2004). Modelling forest transpiration and CO₂ fluxes – Response to soil moisture stress. *Agricultural and Forest Meteorology*, *124*(3–4), 143–156. <https://doi.org/10.1016/j.agrformet.2004.01.007>
- Calvet, J. C., & Soussana, J. F. (2001). Modelling CO₂-enrichment effects using an interactive vegetation SVAT scheme. *Agr. Forest Meteorol.*, *108*, 129–152.
- Canadell, J., Jackson, R. B., Ehleringer, J. R., Mooney, H. A., Sala, O. E., & Schulze, E.-D. (1996). Maximum rooting depth of vegetation types at the global scale. *Oecologia*, *108*(4), 583–595. <https://doi.org/10.1007/BF00329030>
- Canal, N., Calvet, J.-C., Decharme, B., Carrer, D., Lafont, S., & Pigeon, G. (2014). Evaluation of root water uptake in the ISBA-A-gs land surface model using agricultural yield statistics over France. *Hydrology and Earth System Sciences*, *18*, 4979–4999.
- Carrer, D., Meurey, C., Ceamanos, X., Roujean, J.-L., Calvet, J.-C., & Liu, S. (2014). Dynamic mapping of snow-free vegetation and bare soil albedos at global 1km scale from 10-year analysis of MODIS satellite products. *Remote Sensing of Environment*, *140*, 420–432.
- Carrer, D., Roujean, J. L., Lafont, S., Calvet, J. C., Boone, A., Decharme, B., et al. (2013). A canopy radiative transfer scheme with explicit FAPAR for the interactive vegetation model ISBA-A-gs: Impact on carbon fluxes. *Journal of Geophysical Research: Biogeosciences*, *118*, 1–16. <https://doi.org/10.1002/jgrg.20070>
- Charney, J. G., Stone, P. H., & Quirk, W. J. (1975). Drought in the Sahel: A biogeophysical feedback mechanism. *Science*, *187*(4175), 434–435. <https://doi.org/10.1126/science.187.4175.434>
- Ciais, P., Tan, J., Wang, X., Roedenbeck, C., Chevallier, F., Piao, S.-L., et al. (2019). Five decades of northern land carbon uptake revealed by the interhemispheric CO₂ gradient. *Nature*, *568*(7751), 221–225. <https://doi.org/10.1038/s41586-019-1078-6>
- Collatz, G. J., Ball, J. T., Grivet, C., & Berry, J. A. (1991). Physiological and environmental regulation of stomatal conductance, photosynthesis and transpiration: A model that includes a laminar boundary layer. *Agricultural and Forest Meteorology*, *54*(2–4), 107–136. [https://doi.org/10.1016/0168-1923\(91\)90002-8](https://doi.org/10.1016/0168-1923(91)90002-8)
- Collatz, G. J., Ribas-Carbo, M., & Berry, J. A. (1992). Coupled photosynthesis-stomatal conductance model for leaves of C₄ plants. *Australian Journal of Plant Physiology*, *19*, 519–538.
- Dai, M., Yin, Z., Meng, F., Liu, Q., & Cai, W.-J. (2012). Spatial distribution of riverine DOC inputs to the ocean: An updated global synthesis. *Current Opinion in Environment Sustainability*, *4*, 170–178. <https://doi.org/10.1016/j.cosust.2012.03.003>
- De Kauwe, M. G., Medlyn, B. E., Zaehle, S., Walker, A. P., Dietze, M. P., Wang, Y. P., et al. (2014). Where does the carbon go? A model–data intercomparison of vegetation carbon allocation and turnover processes at two temperate forest free-air CO₂ enrichment sites. *New Phytologist*, *203*, 883–899.
- de Noblet-Ducoudré, N., Boisier, J. P., Pitman, A., Bonan, G. B., Brovkin, V., Cruz, F., et al. (2012). Determining robust impacts of land-use-induced land cover changes on surface climate over North America and Eurasia: Results from the first set of LUCID experiments. *Journal of Climate*, *25*(9), 3261–3281. <https://doi.org/10.1175/JCLI-D-11-00338.1>
- Deardorff, J. W. (1977). A parameterization of ground-surface moisture content for use in atmospheric prediction models. *Journal of Applied Meteorology*, *16*(11), 1182–1185. [https://doi.org/10.1175/1520-0450\(1977\)016](https://doi.org/10.1175/1520-0450(1977)016)
- Deardorff, J. W. (1978). Efficient prediction of ground surface temperature and moisture, with inclusion of a layer of vegetation. *Journal of Geophysical Research*, *83*(C4), 1889–1903. <https://doi.org/10.1029/JC083iC04p01889>
- Decharme, B., Brun, E., Boone, A., Delire, C., Le Moigne, P., & Morin, S. (2016). Impacts of snowpack properties and soil organic carbon content on snow characteristics and soil temperature profiles simulated by the ISBA land surface model. *The Cryosphere*, *10*, 853–877. <https://doi.org/10.5194/tc-10-853-2016>
- Decharme, B., Delire, C., Minvielle, M., Colin, J., Vergnes, J.-P., Alias, A., et al. (2019). Recent changes in the ISBA-CTRIP land surface system for use in the CNRM-CM6 climate model and in global off-line hydrological applications. *Journal of Advances in Modeling Earth Systems*, *11*(5), 1207–1252. <https://doi.org/10.1029/2018MS001545>
- Decharme, B., & Douville, H. (2007). Global validation of the ISBA sub-grid hydrology. *Climate Dynamics*, *29*(1), 21–37. <https://doi.org/10.1007/s00382-006-0216-7>
- Delucia, E. H., Drake, J. E., Thomas, R. B., & Gozalez-Meler, M. (2007). Forest carbon use efficiency: Is respiration a constant fraction of gross primary production? *Global Change Biology*, *13*, 1157–1167.
- Domingues, T. F., Martinelli, L. A., & Ehleringer, J. R. (2007). Ecophysiological traits of plant functional groups in forest and pasture ecosystems from eastern Amazonia. *Brazil, Plant Ecol.*, *193*, 101–112.
- FAO/IIASA/ISRIC/ISSCAS/JRC (2012). *Harmonized World Soil Database (version 1.2)*. Rome, Italy and IIASA, Laxenburg, Austria: FAO.
- Faroux, S., Kaptué Tchuenté, A. T., Roujean, J.-L., Masson, V., Martin, E., & Le Moigne, P. (2013). ECOCLIMAP-II/Europe: A twofold database of ecosystems and surface parameters at 1-km resolution based on satellite information for use in land surface, meteorological and climate models. *Geoscientific Model Development*, *6*, 563–582. <https://doi.org/10.5194/gmd-6-563-2013>
- Farquhar, G. D., von Caemmerer, S., & Berry, J. A. (1980). A biochemical model of photosynthetic CO₂ assimilation in leaves of C₃ species. *Planta*, *149*(1), 78–90. <https://doi.org/10.1007/BF00386231>
- Gibelin, A.-L., Calvet, J.-C., Roujean, J.-L., Jarlan, L., & Los, S. (2006). Ability of the land surface model ISBA-A-gs to simulate leaf area index at the global scale: Comparison with satellites products. *Journal of Geophysical Research*, *111*, D18102. <https://doi.org/10.1029/2005JD006691>
- Gibelin, A.-L., Calvet, J. C., & Viovy, N. (2008). Modelling energy and CO₂ fluxes with an interactive vegetation, land surface model, evaluation at high and middle latitudes. *Agricultural and Forest Meteorology*, *148*, 1611–1628.
- Goudriaan, J. (1986). A simple and fast numerical method for the computation of daily totals of crop photosynthesis. *Agricultural and Forest Meteorology*, *38*, 249–254.

- Goudriaan, J., van Laar, H. H., van Keulen, H., & Louwse, W. (1985). Photosynthesis, CO₂ and plant production. In W. Day, & R. K. Atkin (Eds.), *Wheat growth and modelling*, NATO ASI Series, Series A, (Vol. 86, pp. 107–122). New York: Plenum Press.
- Guimberteau, M., Zhu, D., Maignan, F., et al. (2018). ORCHIDEE-MICT (v8. 4.1), a land surface model for the high latitudes: Model description and validation. *Geoscientific Model Development*, *11*, 121–163.
- Hashimoto, S., Carvalhais, N., Ito, A., Migliavacca, M., Nishina, K., & Reichstein, M. (2015). Global spatiotemporal distribution of soil respiration modeled using a global database. *Biogeosciences*, *12*, 4121–4132. <https://doi.org/10.5194/bg-12-4121-2015>
- He, Y., Piao, S. L., Li, X. Y., Chen, A. P., & Qin, D. H. (2018). Global patterns of vegetation carbon use efficiency and their climate drivers deduced from MODIS satellite data and process-based models. *Agricultural and Forest Meteorology*, *256–257*, 150–158. <https://doi.org/10.1016/j.agrformet.2018.03.009>
- Holland, E. A., Matthews, W. M., Post, E., Sulzman, J., Stauffer, R., and Krankina, O. (2015). A global database of litterfall mass and litter pool carbon and nutrients. Data set. Available on-line [<http://daac.ornl.gov>] from Oak Ridge National Laboratory Distributed Active Archive Center, Oak Ridge, Tennessee, USA. <https://doi.org/10.3334/ORNLDAAC/1244>
- Hurttt, G. C., Chini, L. P., Frolking, S., et al. (2011). Harmonization of land-use scenarios for the period 1500–2100: 600 years of global gridded annual land-use transitions, wood harvest, and resulting secondary lands. *Climatic Change*, *109*, 117–161. <https://doi.org/10.1007/s10584-011-0153-2>
- Irmiler, U. (1982). Litterfall and nitrogen turnover in an Amazonian black-water inundation forest. *Plant and Soil*, *67*(1–3), 355–358.
- Ishizaki, S., Hikosaka, K., & Hirose, T. (2003). Increase in leaf mass per area benefits plant growth at elevated CO₂ concentration. *Annals of Botany*, *91*(7), 905–914. <https://doi.org/10.1093/aob/mcg097>
- Jacobs, C. M. J. (1994). Direct impact of atmospheric CO₂ enrichment on regional transpiration, Ph.D. thesis, Agricultural University, Wageningen.
- Joetzjer, E., Delire, C., Douville, H., Ciais, P., Decharme, B., Carrer, D., et al. (2015). Improving the ISBACC land surface model simulation of water and carbon fluxes and stocks over the Amazon Forest. *Geoscientific Model Development*, *8*, 1709–1727. <https://doi.org/10.5194/gmd-8-1709-2015>
- Joetzjer E., Delire C., Douville H., Ciais P., Decharme B., Fisher R., et al. (2014). Predicting the response of the Amazon rainforest to persistent drought conditions under current and future climates: A major challenge for global land surface models, *Geosci. Model Dev.*, *7*, 2933–2950, Dec 2014, doi:<https://doi.org/10.5194/gmd-7-2933-2014>.
- Jung, M. & FLUXCOM team (2016). FLUXCOM (RS + METEO) global land carbon fluxes using CRUNCEP climate data. FLUXCOM Data Portal https://doi.org/10.17871/FLUXCOM_RS_METEO_CRUNCEPv6_1980_2013_v1
- Jung, M., Reichstein, M., & Bondeau, A. (2009). Towards global empirical upscaling of FLUXNET eddy covariance observations: Validation of a model tree ensemble approach using a biosphere model. *Biogeosciences*, *6*, 2001–2013. <https://doi.org/10.5194/bg-6-2001-2009>
- Jung, M., Reichstein, M., Schwalm, C. R., Huntingford, C., Sitch, S., Ahlström, A., et al. (2017). Compensatory water effects link yearly global land CO₂ sink changes to temperature. *Nature*, *541*(7638), 516–520. <https://doi.org/10.1038/nature20780>
- Kattge, J., Diaz, S., Lavorel, S., Prentice, I. C., Leadley, P., Bönlisch, G., et al. (2011). TRY—A global database of plant traits. *Global Change Biology*, *17*, 2905–2935. <https://doi.org/10.1111/j.1365-2486.2011.02451.x>
- Kattge, J., Knorr, W., Raddatz, T., & Wirth, C. (2009). Quantifying photosynthetic capacity and its relationship to leaf nitrogen content for global-scale terrestrial biosphere models. *Global Change Biology*, *15*, 976–991.
- Koronzi, S., McCarty, J., Loboda, T., Kumar, S., & Justice, C. (2006). Global distribution of agricultural fires in croplands from 3 years of Moderate Resolution Imaging Spectroradiometer (MODIS) data. *Global Biogeochem Cycle*, *20*, GB2021. <https://doi.org/10.1029/2005GB002529>
- Koven, C. D., Chambers, J. Q., Georgiou, K., Knox, R., Negron-Juarez, R., Riley, W. J., et al. (2015). Controls on terrestrial carbon feedbacks by productivity versus turnover in the CMIP5 Earth System Models. *Biogeosciences*, *12*, 5211–5228. <https://doi.org/10.5194/bg-12-5211-2015>
- Koven, C. D., Riley, W. J., Subin, Z. M., Tang, J. Y., Torn, M. S., Collins, W. D., et al. (2013). The effect of vertically resolved soil bio-geochemistry and alternate soil C and N models on C dynamics of CLM4. *Biogeosciences*, *10*(11), 7109–7131. <https://doi.org/10.5194/bg-10-7109-2013>
- Krinner, G., Viovy, N., de Noblet-Ducoudré, N., Ogee, J., Polcher, J., Friedlingstein, P., et al. (2005). A dynamic global vegetation model for studies of the coupled atmosphere-biosphere system. *Global Biogeochem Cycle*, *19*(1), 1–33.
- Kucharik, C. J., Foley, J. A., Delire, C., Fisher, V. A., Coe, M. T., Lenters, J. D., Young-Molling, C., et al., (2000). Testing the performance of a dynamic global ecosystem model: Water balance, carbon balance, and vegetation structure. *Global Biogeochemical Cycles*, *14*, 795–825.
- Langerwisch, F., Walz, A., Rammig, A., Tietjen, B., Thonicke, K., & Cramer, W. (2016). Climate change increases riverine carbon outgassing, while export to the ocean remains uncertain. *Earth Syst Dynam*, *7*, 559–582. <https://doi.org/10.5194/esd-7-559-2016>
- Lawrence, P. J., & Chase, T. N. (2010). Investigating the climate impacts of global land cover change in the community climate system model. *International Journal of Climatology*, *30*(13), 2066–2087. <https://doi.org/10.1002/joc.2061>
- Le Quéré, C., Andrew, R. M., Friedlingstein, P., Sitch, S., Hauck, J., Pongratz, J., et al. (2018). Global Carbon Budget 2018. *Earth Syst. Sci. Data*. <https://doi.org/10.5194/essd-10-2141-2018>
- Lin, H. W., McCarty, J. L., Wang, D., Rogers, B. M., Morton, D. C., Collatz, G. J., et al. (2014). Management and climate contributions to satellite-derived active fire trends in the contiguous United States. *Journal of Geophysical Research: Biogeosciences*, *119*, 645–660. <https://doi.org/10.1002/2013JG002382>
- Liu, Y. Y., van Dijk, A. I. J. M., de Jeu, R. A. M., Canadell, J. G., McCabe, M. F., Evans, J. P., & Wang, G. (2015). Recent reversal in loss of global terrestrial biomass. *Nature Climate Change*, *5*. <https://doi.org/10.1038/NCLIMATE258>
- Lloyd, J., & Taylor, J. A. (1994). On the temperature dependence of soil respiration. *Functional Ecology*, *8*, 315–323.
- Malhi, Y., Aragao, L. E. O., Metcalfe, D. B., Paiva, R., Quesada, C. A., Almeida, S., et al. (2009). Comprehensive assessment of carbon productivity, allocation and storage in three Amazonian forests. *Glob. Change Biol.*, *15*, 1255–1274.
- Manabe, S. (1969). Climate and the ocean circulation 1. The atmospheric circulation and the hydrology of the earth's surface. *Mon. Weather Rev.*, *97*(11), 739–774.
- Mangeon, S., Voulgarakis, A., Gilham, R., Harper, A., Sitch, S., & Folberth, G. (2016). INFERNO: A fire and emissions scheme for the UK met office's unified model. *Geoscientific Model Development*, *9*, 2685–2700. <https://doi.org/10.5194/gmd-9-2685-2016>
- Manzoni, S., Capek, P., Porada, P., Thurner, M., et al. (2018). Reviews and syntheses: Carbon use efficiency from organisms to ecosystems —Definitions, theories, and empirical evidence. *Biogeosciences*, *15*, 5929–5949. <https://doi.org/10.5194/bg-15-5929-2018>
- Marschner, B., & Kalbitz, K. (2003). Controls of bioavailability and biodegradability of dissolved organic matter in soils. *Geoderma*, *113*(3–4), 211–235.

- Masson, V., Champeaux, J.-L., Chauvin, F., Meriguet, C., & Lacaze, R. (2003). A global database of land surface parameters at 1-km resolution in meteorological and climate models. *J. Climate*, *16*(9), 1261–1282. <https://doi.org/10.1175/1520-0442>
- Masson, V., Le Moigne, P., Martin, E., Faroux, S., Alias, A., Alkama, R., et al. (2013). The SURFEXv7.2 land and ocean surface platform for coupled or offline simulation of earth surface variables and fluxes. *Geosci. Model Dev*, *6*(4), 929–960. <https://doi.org/10.5194/gmd-6-929-2013-supplement>.
- Mayorga, E., Seitzinger, S. P., Harrison, J. A., Dumont, E., Beusen, A. H. W., Bouwman, A. F., et al. (2010). Global nutrient export from WaterSheds 2 (NEWS2): Model development and implementation. *Environ. Modell.Softw.*, *25*, 837–853.
- McGuire, A. D., Koven, C., Lawrence, D. M., Clein, J. S., Jxia, J., Beer, C., et al. (2016). A model-based analysis of the vulnerability of carbon in the permafrost region between 1960 and 2009. *Global Biogeochemical Cycles*. <https://doi.org/10.1002/2016GB005405>
- Medlyn, B. E., et al. (2015). Using ecosystem experiments to improve vegetation models. *Nature Climate Change*, *5*(6), 528–534. <https://doi.org/10.1038/nclimate262>
- Meinshausen, M., Vogel, E., Nauels, A., Lorbacher, K., Meinshausen, N., Etheridge, D. M., et al. (2017). Historical greenhouse gas concentrations for climate modelling (CMIP6). *Geoscientific Model Development*, *10*, 2057–2116. <https://doi.org/10.5194/gmd-10-2057-2017>
- Mercado, L. M., Lloyd, J., Dolman, A. J., Sitch, S., & Patiño, S. (2009). Modelling basin-wide variations in Amazon forest productivity-Part 1: Model calibration, evaluation and upscaling functions for canopy photosynthesis. *Biogeosciences*, *6*, 1247–1272. <https://doi.org/10.5194/bg-6-1247-2009>
- Monfreda, C., Ramankutty, N., & Foley, J. A. (2008). Farming the planet. Part 2: Geographic distribution of crop areas, yields, physiological types, and net primary production in the year 2000. *Global Biogeochemical Cycles*, GB1022. <https://doi.org/10.1029/2007GB002947>
- Morel, X., Decharme, B., Delire, C., Krinner, G., Lund, M., Hansen, B. U., & Mastepanov, M. (2019). A new process-based soil methane scheme for land surface modeling: Evaluation over arctic field sites with the ISBA land surface model. *Journal of Advances in Modeling Earth Systems*, *11*, 293–326. <https://doi.org/10.1029/2018MS001329>
- Mouillot, F., & Field, C. B. (2005). Fire history and the global carbon budget: A $1^\circ \times 1^\circ$ fire history reconstruction for the 20th century. *Global Change Biology*, *11*(3), 398–420. <https://doi.org/10.1111/j.1365-2486.2005.00920.x>
- NASA LP DAAC, 2017, MOD17A3 Terra/MODIS net primary production yearly L4 global 1 km. NASA EOSDIS Land Processes DAAC, USGS Earth Resources Observation and Science (EROS) Center, Sioux Falls, South Dakota (<https://lpdaac.usgs.gov>), at https://doi.org/10.5067/ASTER/AST_L1T.003.
- Noilhan, J., & Mahfouf, J.-F. (1996). The ISBA land surface parameterization scheme. *Global and Planetary Change*, *13*, 145–159.
- Noilhan, J., & Planton, S. (1989). A simple parameterization of land surface processes for meteorological models. *Monthly Weather Review*. [https://doi.org/10.1175/1520-0493\(1989\)117<0536:ASPOLS>2.0.CO;2](https://doi.org/10.1175/1520-0493(1989)117<0536:ASPOLS>2.0.CO;2)
- Norby, R. J., Warren, J. M., Iversen, C. M., Medlyn, B. E., & McMurtrie, R. E. (2010). CO₂ enhancement of forest productivity constrained by limited nitrogen availability. *Proceedings of the National Academy of Sciences, USA*, *107*, 19,368–19,373.
- Oki, T., & Sud, Y. C. (1998). Design of Total Runoff Integrating Pathways (TRIP)—A global river channel network. *Earth Interactions*, *2*(1), 1–1. <https://doi.org/10.1175/1087-3562>
- Parton, W. J., Stewart, J. W., & Cole, C. V. (1988). Dynamics of C, N, P and S in grassland soils: A model. *Biogeochemistry*, *5*(1), 109–131. <https://doi.org/10.1007/BF02180320>
- Pellegrini, A. F., Ahlström, A., Hobbie, S. E., Reich, P. B., Nieradzik, L. P., Staver, A. C., et al. (2017). Fire frequency drives decadal changes in soil carbon and nitrogen and ecosystem productivity. *Nature*, *553*(7687), 194–198. <https://doi.org/10.1038/nature24668>
- Pielke, R. A., Pitman, A., Niyogi, D., Mahmood, R., McAlpine, C., Hossain, F., et al. (2011). Land use/land cover changes and climate: Modeling analysis and observational evidence. *Wiley Interdisciplinary Reviews: Climate Change*, *2*, 828–850. <https://doi.org/10.1002/wcc.144>
- Pitman, A. J. (2003). The evolution of, and revolution in land surface schemes designed for climate models. *International Journal of Climatology*, *23*(5), 479–510.
- Pitman, A. J., de Noblet-Ducoudré, N., Cruz, F. T., Davin, E. L., Bonan, G. B., Brovkin, V., et al. (2009). Uncertainties in climate responses to past land cover change: First results from the LUCID intercomparison study. *Geophysical Research Letters*, *36*. <https://doi.org/10.1029/2009GL039076>
- Randerson, J. T., Liu, H., Flanner, M. G., Chambers, S. D., Jin, Y., Hess, P. G., et al. (2006). The impact of boreal forest fire on climate warming. *Science*, *314*(5802), 1130–1132. <https://doi.org/10.1126/science.1132075>
- Randerson, J.T., G.R. van der Werf, L. Giglio, G.J. Collatz, and P.S. Kasibhatla. (2017). Global fire emissions database, version 4.1 (GFEDv4). ORNL DAAC, Oak Ridge, Tennessee, USA. <https://doi.org/10.3334/ORNLLDAAC/1293>
- Rawlins, M. A., McGuire, A. D., Kimball, J. K., Dass, P., Lawrence, D., Burke, E., et al. (2015). Assessment of model estimates of land-atmosphere CO₂ exchange across northern Eurasia. *Biogeosciences*, *12*(14), 4385–4405. <https://doi.org/10.5194/bg-12-4385-2015>
- Regnier, P., Friedlingstein, P., Ciais, P., Mackenzie, F. T., Gruber, N., Janssens, I. A., et al. (2013). Anthropogenic perturbation of the carbon fluxes from land to ocean. *Nature Geoscience*, *6*, 597–607. <https://doi.org/10.1038/ngeo1830>
- Resplandy, L., Keeling, R. F., Rödenbeck, C., Stephens, B. B., Khatiwala, S., Rodgers, K. B., et al. (2018). Revision of global carbon fluxes based on a reassessment of oceanic and riverine carbon transport. *Nat. Geosci.*, *11*, 504–509. <https://doi.org/10.1038/s41561-018-0151-3>
- Rocha, A. V., Lorant, M. M., Higuera, P. E., Mack, C. M., Hu, F. S., Jones, B. M., et al. (2012). The footprint of Alaskan tundra fires during the past half-century: implications for surface properties and radiative forcing. *Environmental Research Letters*, *7*, n4. <https://doi.org/10.1088/1748-9326/7/4/044039>
- Saatchi, S. S., Harris, N. L., Brown, S., Lefsky, M., Mitchard, E. T. A., Salas, W., et al. (2011). Benchmark map of forest carbon stocks in tropical regions across three continents. *Proceedings of the National Academy of Sciences of the United States of America*, *108*(24), 9899–9904. <https://doi.org/10.1073/pnas.1019576108>
- Saha, M. V., D'Odorico, P., & Scanlon, T. M. (2017). Albedo changes after fire as an explanation of fire-induced rainfall suppression. *Geophysical Research Letters*, *44*, 3916–3923. <https://doi.org/10.1002/2017GL073623>
- Séférian R., C. Delire, B. Decharme, A. Voldoire, D. Salas y Melia, M. et al. (2016). Development and evaluation of CNRM Earth-System model—CNRM-ESM 1. *Geoscientific Model Development*, *9*, 1423–1453. doi:<https://doi.org/10.5194/gmd-9-1423-2016>.
- Séférian, R., Nabat, P., Michou, M., Saint-Martin, D., Voldoire, A., Colin, J., et al. (2019). Evaluation of CNRM earth system model, CNRM-ESM 2-1: Role of Earth System processes in present-day and future climate. *Journal of Advances in Modeling Earth Systems*, *11*, 4182–4227. <https://doi.org/10.1029/2019MS001791>
- Sitch, S., Smith, B., Prentice, I. C., et al. (2003). Evaluation of ecosystem dynamics, plant geography and terrestrial carbon cycling in the LPJ dynamic vegetation model. *Global Change Biology*, *9*, 161–185. <https://doi.org/10.1046/j.1365-2486.2003.00569.x>
- Stocker, B. D., Feissli, F., Strassmann, K. M., Spahni, R., & Joos, F. (2014). Past and future carbon fluxes from land use change, shifting cultivation and wood harvest. *Tellus B: Chemical and Physical Meteorology*, *66*, 1. <https://doi.org/10.3402/tellusb.v66.23188>

- Thonicke, K., Venevsky, S., Sitch, S., & Cramer, W. (2001). The role of fire disturbance for global vegetation dynamics: Coupling fire into a dynamic global vegetation model. *Global Ecol Biogeographica*, *10*, 661–677.
- Thurner, M., Beer, C., Santoro, M., Carvalhais, N., Wutzler, T., Schepaschenko, D., et al. (2014). Carbon stock and density of northern boreal and temperate forests. *Global Ecology and Biogeography*, *23*, 297–310. <https://doi.org/10.1111/geb.12125>
- Tramontana, G., Jung, M., Schwalm, C. R., Ichii, K., Camps-Valls, G., Ráduly, B., et al. (2016). Predicting carbon dioxide and energy fluxes across global FLUXNET sites with regression algorithms. *Biogeosciences*, *13*, 4291–4313. <https://doi.org/10.5194/bg-13-4291-2016>
- van der Werf, G. R., Randerson, J. T., Giglio, L., van Leeuwen, T. T., Chen, Y., Rogers, B. M., et al. (2017). Global fire emissions estimates during 1997–2016. *Earth System Science Data*, *9*, 697–720. <https://doi.org/10.5194/essd-9-697-2017>
- Van Heemst, H. D. J. (1986). Potential crop production. In H. Van Keulen & J. Wolf (Eds.), *Modelling of Agricultural Production: Weather, Soil and Crops. Simulation Monographs*. Pudoc, Wageningen.
- Vergnes, J.-P., & Decharme, B. (2012). A simple groundwater scheme in the TRIP river routing model: Global off-line evaluation against GRACE terrestrial water storage estimates and observed river discharges. *Hydrology and Earth System Sciences*, *16*(10). <https://doi.org/10.5194/hess-16-3889-2012>
- Viovy, N. (2018). CRUNCEP Version 7—Atmospheric Forcing Data for the Community Land Model. Boulder, CO: Research Data Archive at the National Center for Atmospheric Research, Computational and Information Systems Laboratory. Retrieved from <http://rda.ucar.edu/datasets/ds314.3/>
- Voldoire, A., Sanchez-Gomez, E., Salas y Méria, D., Decharme, B., Cassou, C., Sénési, S., et al. (2013). The CNRM-CM5.1 global climate model: Description and basic evaluation. *Climate Dynamics*, *40*(9–10), 2091–2121. <https://doi.org/10.1007/s00382-011-1259-y>
- Wetterstedt, M. (2010). Decomposition of soil organic matter. Diss. (sammanfattning/summary) Uppsala : Sveriges lantbruksuniversitet. *Acta Universitatis Agriculturae Sueciae*, 1652-6880, 2010:21 ISBN 978-91-576-7498-2 [Doctoral thesis].
- Wu, D., Piao, S., Liu, Y., Ciais, P., & Yao, Y. (2018). Evaluation of CMIP5 Earth System Models for the Spatial Patterns of Biomass and Soil Carbon Turnover Times and Their Linkage with Climate. *Journal of Climate*, *31*, 5947–5960. <https://doi.org/10.1175/JCLI-D-17-0380.1>
- Xia, J., McGuire, A., Lawrence, D., Burke, E., Chen, G., Chen, X., et al. (2017). Terrestrial ecosystem model performance in simulating productivity and its vulnerability to climate change in the northern permafrost region. *Journal of Geophysical Research: Biogeosciences*, *122*, 430–446. <https://doi.org/10.1002/2016JG003384>
- Yin, X. (2002). Responses of leaf nitrogen concentration and specific leaf area to atmospheric CO₂ enrichment: A retrospective synthesis across 62 species. *Global Change Biology*, *8*, 631–642. <https://doi.org/10.1046/j.1365-2486.2002.00497.x>
- Zhang, Y. J., Yu, G. R., Yang, J., Wimberly, M. C., Zhang, X. Z., Tao, J., et al. (2014). Climate-driven global changes in carbon use efficiency. *Global Ecology and Biogeography*, *23*, 144–155. <https://doi.org/10.1111/nph.13978>
- Zhao, M., Heinsch, F. A., Nemani, R. R., & Running, S. W. (2005). Improvements of the MODIS terrestrial gross and net primary production global data set. *Remote Sensing of Environment*, *95*, 164–176.
- Zhu, Z., Bi, J., Pan, Y., Ganguly, S., Anav, A., Xu, L., et al. (2013). Global data sets of vegetation Leaf Area Index (LAI)3g and Fraction of photosynthetically Active Radiation (FPAR)3g derived from Global Inventory Modeling and Mapping Studies (GIMMS) Normalized Difference Vegetation Index (NDVI)3g for the period 1981 to 2011. *Remote Sensing*, *5*(2), 927–948. <https://doi.org/10.3390/rs50209275>